Published in final edited form as:
J Am Chem Soc. 2010 December 8; 132(48): 17118–17129. doi:10.1021/ja1045428.

Sulfur versus Iron Oxidation in an Iron-Thiolate Model Complex

Aidan R. McDonald[a], **Michael R. Bukowski**[a,e], **Erik R. Farquhar**[a], **Timothy A. Jackson**[a,f], **Kevin D. Koehntop**[a], **Mi Sook Seo**[b], **Raymond F. De Hont**[c], **Audria Stubna**[c], **Jason A. Halfen**[d], **Eckard Münck**[c,*], **Wonwoo Nam**[b,*], and **Lawrence Que Jr.**[a,*]

[a]Department of Chemistry and Center for Metals in Biocatalysis, 207 Pleasant Street S.E., University of Minnesota, Minneapolis, MN 55455

[b]Department of Bioinspired Science, Department of Chemistry and Nano Science, Center for Biomimetic Systems, Ewha Womans University, Seoul 120-750, Korea

[c]Department of Chemistry, Carnegie Mellon University, Mellon Institute, 4400 Fifth Ave., Pittsburgh, PA 15213

[d]Department of Chemistry, University of Wisconsin-Eau Claire, 443 Phillips Hall, Eau Claire, WI 54702

Abstract

In the absence of base, the reaction of $[Fe^{II}(TMCS)]PF_6$ (**1**, TMCS = 1-(2-mercaptoethyl)-4,8,11-trimethyl-1,4,8,11-tetraazacyclotetradecane**)** with peracid in methanol at −20 °C did not yield the oxoiron(IV) complex (**2**, $[Fe^{IV}(O)(TMCS)]PF_6$), as previously observed in the presence of strong base (KO^tBu). Instead, the addition of one equivalent of peracid resulted in 50% consumption of **1**. The addition of a second equivalent of peracid resulted in the complete consumption of **1**, and the formation of a new species **3** as monitored by UV-Vis, ESI-MS and Mössbauer spectroscopies. ESI-MS showed **3** to be formulated as $[Fe^{II}(TMCS) + 2O]^+$), while EXAFS analysis suggested that **3** was an O-bound iron(II)-sulfinate complex (Fe–O = 1.95 Å, Fe–S = 3.26 Å). The addition of a third equivalent of peracid resulted in the formation of yet another compound, **4**, which showed electronic absorption properties typical of an oxoiron(IV) species. Mössbauer spectroscopy confirmed **4** to be a novel iron(IV) compound, different from **2**, and EXAFS (Fe=O = 1.64 Å) and resonance Raman ($\nu_{Fe=O}$ = 834 cm^{-1}) showed that indeed an oxoiron(IV) unit had been generated in **4**. Furthermore, both infra-red and Raman spectroscopy gave indications that **4** contains a metal-bound sulfinate moiety ($\nu_s(SO_2)$ = ~ 1000 cm^{-1}, $\nu_{as}(SO_2)$ = ~ 1150 cm^{-1}). Investigations into the reactivity of **1** and **2** towards H^+ and oxygen atom transfer reagents have led to a mechanism for sulfur oxidation in which **2** could form even in the absence of base, but is rapidly protonated to yield an oxoiron(IV) species with an uncoordinated thiol moiety that acts as both oxidant and substrate in the conversion of **2** to **3**.

1. Introduction

Thiolate ligation plays a vital role in a wide variety of iron-containing enzymes involved in the activation of dioxygen and deactivation of reactive oxygen species (ROS). In cytochrome P450, the highly donating axial Cys ligand acts to facilitate heterolytic cleavage

larryque@umn.edu, wwnam@ewha.ac.kr, emunck@cmu.edu.
[e]Current address: Department of Chemistry, Penn State Altoona, Altoona, PA 1660
[f]Current address: Department of Chemistry, University of Kansas, Lawrence, KS 66045

Supporting Information Available. Iron K-edge XANES and EXAFS data and fitting analyses for compounds **1, 3, 4**, and **6**. FT-IR spectra of compounds **3, 6** and $[Zn^{II}(TMCSO_2)]^+$. Mössbauer spectrum of compound **6**. Extended Scheme 3. This material is available free of charge via the Internet at http://pubs.acs.org.

of an O–O bond in a Fe^{III}–OOH precursor to form Compound I $[(L^{+\bullet})Fe^{IV}=O]^{+}$ (L = porphyrin).1,2 In contrast, for superoxide reductase (SOR), which contains a *non-heme* iron center with four equatorial His ligands and an axial Cys, the thiolate acts to stabilize the O–O bond of a peroxoiron(III) intermediate and to weaken the Fe–O_2 bond to facilitate dissociation of H_2O_2.3 For both cysteine dioxygenase (CDO) and isopenicillin N synthase (IPNS) the substrate thiolate ligates *cis* to the O_2 binding site and becomes primed for oxidation. CDO catalyzes the conversion of cysteine to cysteinesulfinate.4 It is proposed that dioxygen reacts with the cysteinyl thiolate-bound iron(II) center in CDO forming a superoxoiron(III)-cysteinate intermediate, which converts to a persulfenate intermediate and ultimately an S-bound iron(II)-cysteinesulfinate.5 IPNS catalyzes the oxidation of the thiolate-containing tripeptide substrate to the isopenicillin product containing a thiazolidine ring in a two-step process involving superoxoiron(III) and oxoiron(IV) oxidants.6 With a substrate analog, the thiol function can instead be oxidized to sulfenate.7 Lastly, iron(III) and cobalt(III) nitrile hydratases (NHase) have active sites where two of the three Cys ligands are oxidized to sulfenate and sulfinate that are S-bound to the metal center.8 The maturation of the NHase active site occurs post-translationally9 and presumably by metal-assisted oxidation.

Recent biomimetic efforts have focused on modeling the iron-thiolate chemistry of SOR and NHase.10 In efforts to model putative peroxo intermediates of SOR, $[Fe^{III}(SR)(OOH(R))]$ complexes were characterized by several groups.11 In these studies there was little mention of any oxidation byproducts involving the thiolate sulfur. In efforts to mimic the active site of NHase, thiolatoiron(III) or -cobalt(III) complexes were found to be oxidized to derivatives with S-bound sulfenate and/or sulfinate ligands as found in the enzymes. Artaud reported a bis(thiolate)iron(III) complex that reacted with O_2 to form an S-bound bis(sulfinato)iron(III) complex.12 The same group showed that selective sulfur oxidation of a dithiol ligand can occur prior to metal (cobalt(III)) insertion, suggesting that metal-mediated oxidation may *not* necessarily be involved in NHase.13 Kovacs found iron(III) and cobalt(III) di- and tri-thiolate complexes that reacted readily with O_2 to form a variety of O- and S-bound metal(III)-sulfenate and -sulfinate species.14 Grapperhaus demonstrated that the spin-state of iron(III)-thiolate complexes can modulate the reactivity of bound thiolate to dioxygen.15 Goldberg has recently reported an iron(II)-thiolate complex that was converted to an iron(II)-sulfonate complex upon exposure to O_2, demonstrating the first functional mimic of CDO.16 The analogous zinc(II)-thiolate complex showed no reactivity towards O_2, implicating the iron site in sulfur oxidation. Heme iron(III)-thiolate model complexes have, in some cases, also been found to react with oxidants to yield axial iron(III)-sulfonate complexes.17 Unfortunately, very little insight into the mechanism of sulfur oxidation in all of these model complexes was obtained. One mass spectrometry study into the reaction of an iron(III)-thiolate and dioxygen identified intermediate species to be iron(III)-sulfenate, which over time was converted to iron(III)-sulfinate.18

In the course of our work on synthetic high-valent iron complexes, we investigated the reaction of $[Fe^{II}(TMCS)]^{+}$ (**1**, TMCS = 1-(2-mercaptoethyl)-4,8,11-trimethyl-1,4,8,11-tetraazacyclotetradecane, Scheme 1) with 3-chloroperoxybenzoic acid (*m*-CPBA). In the presence of strong base, this reaction generates **2**, an oxoiron(IV) complex with a thiolate ligand *trans* to the oxo- group that is the only synthetic complex thus far to model the RS-Fe^{IV}=O unit associated with the active oxidants of cytochrome P450 and chloroperoxidase.1,19 Complex **2** belongs to a growing family of oxoiron(IV) complexes supported by non-porphyrin ligands,20 including TMC21 (TMC = 1,4,8,11-tetramethyl-1,4,8,11-tetraazacyclotetradecane, Scheme 1), TPA22 (TPA = tris(2-pyridylmethyl)amine, Scheme 1), and N4Py23 (N4Py = N,N-bis(2-pyridylmethyl) N-bis(2-pyridyl)methylamine, Scheme 1). The presence of the thiolate ligand *trans* to the oxo group enhanced the H-atom abstraction reactivity of the Fe=O unit but diminished its oxo-transfer ability.21(c)

Herein we show that, in the *absence* of base, **1** is rapidly converted upon exposure to two equivalents of peracid to an S-oxidized species [$Fe^{II}(TMCSO_2)$] (**3**), which can further be oxidized to [$Fe^{IV}(O)(TMCSO_2)$] (**4**) with the addition of a third equivalent of peracid. Both new species have been extensively characterized, with the sulfinate functionality likely to be O-bound to the iron center. Experiments probing the mechanism of sulfur oxidation are presented and show that the oxoiron(IV) moiety of **2** could be involved in the oxidation of thiolate to sulfinate.

2. Experimental

Materials

All reagents and solvents were purchased from commercial sources and used as received, unless otherwise stated. All reactions with air-sensitive materials were conducted under an inert atmosphere using either standard Schlenk techniques or in a glove box. Methanol was purified by refluxing over metallic magnesium and subsequent distillation. 1-(2-mercaptoethyl)-4,8,11-trimethyl-1,4,8,11-tetraazacyclotetradecane (TMCSH) and its iron(II) complex (**1**, [$Fe^{II}(TMCS)]PF_6$) were synthesized according to literature procedures.[24,25] ^{57}Fe-enriched **1** was synthesized using the same procedure but with $^{57}Fe(OTf)_2(NCCH_3)_2$ as the source of Fe. 3-Chloroperoxybenzoic acid (77% Aldrich, *m*-CPBA) was purified according to literature procedures (titrated iodometrically, 85% pure).[26]

Preparation of Intermediates 3 and 4

The preparation of intermediates **3** and **4** was carried out under an inert gas atmosphere. Intermediate **3** was prepared by the addition of 2 equivalents of *m*-CPBA to a stirring solution of **1** (1 mM, MeOH) at −20 °C. Intermediate **4** was prepared by addition of 3 equivalents of *m*-CPBA to a stirring solution of **1** (1 mM, MeOH) at −20 °C. Both intermediates **3** and **4** were stable at −20 °C, but intermediate **4** reacted further upon warming to room temperature. Intermediate **3** was stable at room temperature.

Preparation of [$Fe^{II}(TMC)(O_2SPh)_2$] (6)

The preparation of **6** was carried out under an inert gas atmosphere. 0.290 g (2.29 mmol) $FeCl_2$ and 0.590 g (2.29 mmol) 1,4,8,11-tetramethyl-1,4,8,11-tetraazacyclotetradecane (TMC) were mixed together in MeOH (5 mL) for one hour. 0.750 g (4.58 mmol) sodium benzenesulfinate was added and the resulting solution was stirred at room temperature for 2 days. MeOH was removed *in vacuo*, and the resulting oily solid was dissolved in CH_2Cl_2 and filtered over celite. Subsequent recrystalization from CH_2Cl_2/Et_2O (2x) yielded the desired product as a colorless crystalline material. Yield 60%. Anal. Calcd. for $C_{26}H_{42}O_4N_4S_2Fe$: C, 52.52; H, 7.12; N, 9.42; Found: C, 52.01; H, 7.24; N, 9.45. ESI-MS Calcd. for $C_{26}H_{42}O_4N_4S_2Fe$ 594.20; Found 453.30 (loss of one sulfinate [$Fe^{II}(TMC)(O_2SPh)]^+$). ^{1}H NMR (acetone-d_6, 300 MHz): δ = −9.5, −8.7, −6.7, −4.5, 1.1, 3.4, 5.5, 6.6, 9.4, 10.7, 12.9, 44, 57, 75, 109, 113, 271, 281.

Preparation of [$Zn^{II}(TMCS)]PF_6$ (7)

Zinc complex **7** was synthesized using the same procedure as reported for the synthesis of iron complex **1**.[24] 1-(2-mercaptoethyl)-4,8,11-trimethyl-1,4,8,11-tetraazacyclotetradecane (0.2 g, 0.66 mmol) and LiOH (0.016 g, 0.66 mmol) were mixed at room temperature in MeOH (3 mL) for 1 hour. $Zn(OTf)_2$ (0.24 g, 0.66 mmol) was then added and the resulting mixture was stirred for 1 hour at room temperature and subsequently filtered over Celite. $NaPF_6$ (0.44 g, 2.6 mmol) in MeOH (3 mL) was then added, resulting in the precipitation of a white crystalline material that was then collected by vacuum filtration. Recrystalization

from CH_2Cl_2/Et_2O yielded the desired product in 55% yield. Anal. Calcd. for $[Zn^{II}(TMCS)CH_3CN]PF_6.2CH_2Cl_2$ ($C_{19}H_{40}Cl_4F_6N_5PSZn$): C, 31.57; H, 5.58; N, 9.69; Found: C 31.26, H 5.70, N 9.08. ESI-MS Calcd. for $C_{15}H_{33}F_6N_4PSZn$ 365.17; Found 365.17 (loss of PF_6 $[Zn^{II}(TMCS)]^+$). ^1H NMR (DMSO-d_6, 300 MHz): δ = 1.52 (t, 2H), 1.80 (m, 2H), 2.10 – 2.35 (m, 9H), 2.39 (s, 3H), 2.41 (s, 3H), 2.55- 3.0 (br m, 8H) 3.0 −3.3 (br m, 6H).

Reactivity Studies

Kinetic studies on the oxidative reactivity of **4** were performed by adding varying amounts of either triphenylphosphine (PPh_3) or dihydroanthracene (DHA) to a solution of **4** in $MeOH/CH_3CN$ (1:1). Rate constants (k_{obs}) were determined by pseudo-first-order fitting of the disappearance of the electronic absorption band at 830 nm. The second order rate constants (k_2) were determined by plotting k_{obs} versus [substrate].21(c) Product analysis for the oxidation of PPh_3 was done using ^{31}P NMR. Product analysis for the oxidation of DHA was done using UV-vis spectroscopy and GCMS.

X-ray crystal structure determination of 6

A crystal (approximate dimensions 0.45× 0.42 × 0.08mm) was placed onto the tip of a 0.1 mm diameter glass capillary and mounted on a CCD area detector diffractometer for data collection at 173(2) K.27 A preliminary set of cell constants was calculated from reflections harvested from three sets of 20 frames. These initial sets of frames were oriented such that orthogonal wedges of reciprocal space were surveyed. This produced initial orientation matrices determined from 104 reflections. The data collection was carried out using Mo Kα radiation (graphite monochromator) with a frame time of 20 seconds and a detector distance of 4.9 cm. A randomly oriented region of reciprocal space was surveyed to the extent of one sphere and to a resolution of 0.80 Å. Four major sections of frames were collected with 0.30° steps in ω at four different ϕ settings and a detector position of −28° in 2θ. The intensity data were corrected for absorption and decay (SADABS).28 Final cell constants were calculated from 2899 strong reflections from the actual data collection after integration (SAINT).29 Refer to Table 1 for additional crystal and refinement information. The structure was solved using Bruker SHELXTL and refined using Bruker SHELXTL.30 The space group $P2_12_12_1$ was determined based on systematic absences and intensity statistics. A direct-methods solution was calculated which provided most non-hydrogen atoms from the E-map. Full-matrix least squares/difference Fourier cycles were performed which located the remaining non-hydrogen atoms. All non-hydrogen atoms were refined with anisotropic displacement parameters. All hydrogen atoms were placed in ideal positions and refined as riding atoms with relative isotropic displacement parameters. The final full matrix least squares refinement converged to $R1 = 0.0382$ and $wR2 = 0.0798$ (F^2, all data).

Physical Methods

Electronic absorption spectra were recorded on a Hewlett-Packard (Agilent) 8453 diode array spectrophotometer (190–1100-nm range) in quartz cuvettes cooled using a liquid nitrogen cooled cryostat from Unisoku Scientific Instruments (Osaka, Japan). Mössbauer spectra were recorded with two spectrometers, using Janis Research Super-Varitemp dewars that allowed studies in applied magnetic fields up to 8.0 T in a temperature range of 1.5 to 200 K. Mössbauer spectral simulations were performed using the WMOSS software package (WEB Research, Edina, MN). Isomer shifts are quoted relative to Fe metal at 298 K. High-resolution electrospray mass spectrometry was performed using a Bruker Bio-TOF II spectrometer. Metastable species were infused directly into the instrument using a pre-chilled gas-tight syringe. Fourier transform infra-red transmission spectra were recorded at room temperature on a solid sample, on a Thermo-Nicolet Avatar 370 FT-IR. Resonance

Raman spectra were collected on an ACTON AM-506M3 monochromator with a Princeton LN/CCD data collection system using a Spectra-Physics Model 2060 krypton laser. All measurements were carried out on frozen solutions at 77 K with ~10 mW power at the samples. Samples were frozen onto a gold-plated copper cold-finger in thermal contact with a Dewar flask containing liquid nitrogen. Raman shifts were calibrated with indene (accuracy ± 1 cm^{-1}).

XAS Data Collection

X-ray absorption spectroscopic data for **3** was collected on beamline X9B of the National Synchrotron Light Source (NSLS) at Brookhaven National Laboratory, with storage ring conditions of 2.8 GeV and 100 – 300 mA, while data for **1, 4**, and **6** were collected on beamline 7-3 of the Stanford Synchrotron Radiation Lightsource (SSRL) of SLAC National Accelerator Laboratory with storage ring conditions of 3.0 GeV and 80 – 100 mA. At NSLS, Fe K-edge XAS data were collected for a frozen solution of **3** (in MeOH, 6 complete scans) maintained at *ca.* 15 K over an energy range of 6.9 – 8.0 keV using a Si(111) double crystal monochromator for energy selection and a Displex closed cycle cryostat for temperature control. A bent focusing mirror was used for harmonic rejection. The sample of **3** studied by XAS contained 14 mM Fe; Mössbauer analysis indicated a yield for **3** of 75%, with the balance of the sample consisting of **4** (11%) and an iron(III) species (14%). At SSRL, Fe K-edge XAS data were collected for frozen solutions of **1** (in MeCN, 40 mM $[Fe]_T$, 4 complete scans), **4** (in MeCN, 8.0 mM $[Fe]_T$, 80% iron(IV) by UV/Vis, 14 complete scans), and **6** (in THF, 30 mM $[Fe]_T$, 4 complete scans) maintained at a temperature of *ca.* 10 K over an energy range of 6.9 – 8.0 keV using a Si(220) double crystal monochromator for energy selection and an Oxford Instruments CF1208 continuous flow liquid helium cryostat for temperature control. Harmonic rejection was achieved by a 9 keV cutoff filter. Data were obtained as fluorescence excitation spectra with either a 13-element (NSLS) or 30-element (SSRL) solid-state germanium detector array (Canberra). An iron foil spectrum was recorded concomitantly for internal energy calibration and the first inflection point of the K-edge was assigned to 7112.0 eV.

XAS Data Analysis

Data reduction, averaging, and normalization were performed using the program EXAFSPAK.31 Following calibration and averaging of the data, background absorption was removed by fitting a Gaussian function to the pre-edge region and then subtracting this function from the entire spectrum. A three-segment spline with fourth order components was then fit to the EXAFS region of the spectrum in order to extract $\chi(k)$. Analysis of the pre-edge features was carried out with the program SSExafs32 using a previously described protocol.33 Theoretical phase and amplitude parameters for a given absorber-scatterer pair were calculated using FEFF 8.4034 at the single-scattering level of theory, and were utilized by the opt program of the EXAFSPAK package during curve-fitting. Parameters for **1** were calculated using the coordinates of the crystal structure reported.25 Parameters for **3** were calculated for a modification of the starting complex structure in which an O-bound sulfinate was introduced, such that the Fe•••S distance was increased to 3.3 Å from the 2.3 Å distance in **1** and an O atom bound to the sulfur was placed at a distance of 2.0 Å from the Fe center. The Fe–O–S bond angle was ~130°. These parameters are consistent with other iron(II)-sulfinate moieties that have been described in the literature.41,42 Parameters for **4** were calculated for a modification of the DFT structure published for **2** in which an O-bound sulfinate was introduced, such that the Fe•••S distance was increased to 3.3 Å and an O atom bound to the sulfur was placed at a distance of 2.0 Å from the Fe center. The Fe–O–S bond angle was ~130°. The Fe=O bond length was adjusted to 1.64 Å. A path for a Fe–S interaction at 2.3 Å (as seen in the crystal structure of **1** and the EXAFS analysis of **2**) was also considered in order to test a wider range of possible Fe•••S distances. Finally,

parameters for **6** were calculated using the coordinates of the crystal structure reported in this work (*vide infra*). Structures of the models for **3, 4**, and **6** are shown in Figure S1 of the Supporting Information. In all analyses, the coordination number of a given shell was a fixed parameter, and was varied iteratively while bond lengths (*r*) and Debye-Waller factors (σ^2) were allowed to freely float. The amplitude reduction factor S0 was fixed at 0.9, while the edge shift parameter E0 was allowed to float as a single value for all shells (thus in any given fit, the number of floating parameters = (2 × num shells) + 1).). The goodness of fit, F (or *F*-factor) was defined as $[\Sigma k^6(\chi_{exptl}-\chi_{calc})^2 / \Sigma k^6 \chi_{exptl}^2]^{1/2}$.

3. Results and Discussion

3.1 Identifying Intermediates - Defining the reaction landscape

3.1.1 Electronic Absorption Spectroscopy—The iron(II) complex of the macrocyclic ligand TMCS (**1**, $[Fe^{II}(TMCS)(PF_6)]$, Scheme 1) dissolved in anhydrous, anaerobic methanol (MeOH) exhibits an electronic absorption spectrum with an intense UV feature at λ_{max} = 320 nm (ε = 1500 $M^{-1}cm^{-1}$), previously assigned to a thiolate-to-iron(II) charge transfer transition.25 The addition of *one* equivalent of 3-chloroperoxybenzoic acid (*m*-CPBA) to **1** at −20 °C showed the rapid (1 min.) consumption (approximately 50%, see Figures 1 and 2) of the λ_{max} = 320 nm band, with no features appearing in the visible or near-IR regions of the absorption spectrum. The addition of a *second* equivalent of *m*-CPBA resulted in the complete consumption of the λ_{max} = 320 nm feature (1 min.) and the appearance of a new shoulder at λ_{max} = 280 nm (ε = 3000 $M^{-1}cm^{-1}$) that is associated with the oxidation product **3**. From Figure 2 the stoichiometry of the conversion of **1** to **3** can be deduced. The addition of 0.5, 1, and 1.5 equivalents of *m*-CPBA showed a linear decrease of the λ_{max} = 320 nm feature, suggesting rapid and quantitative conversion of **1** to **3**. After addition of 1.5 equivalents of *m*-CPBA, new features in the UV region appear, and hence the trace of the λ_{max} = 320 nm feature shows an increase in Figure 2. The new, feature arises from an oxoiron(IV) complex discussed below, but evidence for the formation of this high-valent iron species was not observed prior to the addition of 1.5 or more equivalents of peracid. We surmise that the reaction of **1** with 2 equivalents *m*-CPBA yields another low-valent iron complex. The thiolate sulfur is the mostly likely site of oxidation apart from the iron(II) center in **1**, and the stoichiometry would suggest that the thiolate is converted to a sulfinate - a stable moiety at low temperatures.

The addition of a *third* equivalent of *m*-CPBA to the solution resulted in the gradual formation of oxoiron(IV) complex, **4**, over 30 minutes with spectral features at λ_{max} = 330 nm (ε = 9000 $M^{-1}cm^{-1}$), λ_{max} = 830 nm (ε = 170 $M^{-1}cm^{-1}$) and 990 nm (ε = 170 $M^{-1}cm^{-1}$). Near-IR transitions are found that are characteristic of d-d transitions in $S = 1$ $[Fe^{IV}(O)(L)]$ complexes.35 The observed “double-humped” near-IR features resemble those of $[Fe^{IV}(O)(TMC)(X)]$ complexes where X is a weakly basic anion like $-O_2CCF_3$.21(d) Both species **3** and **4** were stable at −20 °C,36 but intermediate **4** decomposed over a period of hours when warmed to room temperature. Apparently iron oxidation is preferential to sulfur oxidation in the reaction of **3** with peracid, suggesting that the low-valent iron sulfinate **3** is converted to an oxoiron(IV) sulfinate, **4**, when the third equivalent of peracid is added to the reaction mixture. Scheme 2 depicts the proposed stepwise conversion of iron(II)-thiolate **2** to iron(II)-sulfinate **3** and subsequently oxoiron(IV)-sulfinate **4**, as well as the conversion of **1** to **2** in the presence of base.

3.1.2 Mössbauer spectroscopy—Mössbauer spectroscopy gave insights into the iron oxidation states of intermediates **3** and **4**. Complex **1** displayed Mössbauer parameters typical of a high-spin iron(II) complex (δ = 0.90 mm/s, ΔE_Q = 3.06 mm/s, Figure 3A, Table 2).37 The Mössbauer spectrum observed when one equivalent of *m*-CPBA was added to **1**

showed the formation of a new high-spin iron(II) species (**3**, 50%, δ = 1.06 mm/s, ΔE_Q = 3.77 mm/s), along with unreacted **1** (50%). The addition of a second equivalent of oxidant showed formation of **3** in 92% yield with 8% of the iron present belonging to an iron(IV) species (**5**, δ = 0.16 mm/s, ΔE_Q = 1.15 mm/s, Figure 3C). We assign **5** to be a transient precursor to **4**, which is discussed in greater detail in section 3.2. The conversion of **1** to **3** is thus clean and rapid, and indicates that indeed the reaction between **1** and 2.0 equivalents peracid is likely purely a ligand modification reaction. The change in isomer shift on going from **1** to **3** and the increase in quadrupole splitting (Table 2) are both consistent with the replacement of the thiolate in **1** with a much less basic axial ligand, putatively a sulfinate.

Complex **4**, observed upon addition of a third equivalent of peracid, exhibited Mössbauer parameters typical of an iron(IV) species (δ = 0.19 mm/s, ΔE_Q = 1.28 mm/s), confirming the UV-Vis diagnosis (Figure 3D). Furthermore, the yield of **4** was found to be almost quantitative (86% Fe^{IV}). The observed isomer shift (δ) compares favorably with results observed for analogous [Fe^{IV}(O)(TMC)(X)] complexes, which generally show values in the range 0.15 – 0.20 mm/s.21(d) More importantly, the large quadrupole splitting (ΔE_Q) gives a good indication as to the electronic nature of the axial ligand, as the value of ΔE_Q for **4** is comparable to those found for axial $NCCH_3$ (ΔE_Q = 1.24 mm/s) and $^-O_2CCF_3$ (ΔE_Q = 1.39 mm/s) ligands, but much larger than those associated with more basic axial ligands (e.g. ^-SR, ΔE_Q = −0.22 mm/s; ^-CN, ΔE_Q = 0.25 mm/s). This difference reflects low electronic symmetry around the iron center, consistent with the presence of a weakly basic axial ligand.

3.1.3 Mass Spectrometry—Low temperature electrospray ionization mass spectrometry (ESI-MS) provides evidence for the elemental compositions of intermediates **3** and **4** (Figure 4). The addition of one equivalent of *m*-CPBA to **1** ([Fe^{II}(TMCS)]$^+$, *m/z* = 357.1) showed the formation of a peak at *m/z* = 389.2 of comparable intensity to that of residual **1**, indicating the incorporation of two oxygen atoms for 3 ([Fe^{II}(TMCS(O)2]$^+$). Addition of a second equivalent of *m*-CPBA showed a significant decrease in intensity of the peak corresponding to **1** relative to that of the *m/z* = 389.2 mass peak (**3**). Peaks corresponding to **4** were observed after the addition of 2 equivalents of oxidant (*m/z* = 405.2, [Fe^{IV}(TMCS)$(O)_3$]$^+$).38 These results together with the Mössbauer data further corroborate the proposed formation of a sulfinate, demonstrating the incorporation of two oxygen atoms into **1** to generate **3**, an iron(II)-sulfinate. As can be seen in Figure 4, no evidence for a species incorporating one oxygen atom was observed (**2**, *m/z* = 373.1) in the conversion of **1** to **3**. This would suggest the conversion from **1** to **3** is rapid and clean, with any putative sulfenate intermediate very short-lived.

The addition of the third equivalent of oxidant resulted in the appearance of a dominant peak at *m/z* = 405.2 ([Fe^{IV}(TMCS)$(O)_3$]$^+$), which we have assigned to be **4**, and much less intense features at 357.1 (**1**) and 389.2 (**3**). Combining this observation with the spectral features observed upon addition of a third equivalent of oxidant to **1**, we conclude that **4** is most likely an oxoiron(IV) sulfinate complex. There was some evidence for [Fe^{IV}(TMCS)$(O)_4$]$^+$ in the mass analysis of **4**, but the relative intensity of the peak was small.38

3.1.4 Vibrational Spectroscopy—Methods to probe vibrational modes proved useful in providing additional insight into the location of the three oxygen atoms incorporated into **1** to make **4**. Resonance Raman evidence for an oxoiron(IV) unit using 406.7-nm excitation revealed an enhanced band at 831 cm^{-1} typical of an Fe=O stretch (Figure 5). The observed stretching frequency, together with the observed Mössbauer quadrupole splitting and X-ray absorption pre-edge area (Table 1), suggests the presence of a weak axial donor ligand comparable to CH_3CN in basicity, as correlated for a series of [Fe^{IV}(O)(TMC)(X)]

complexes.39 Unfortunately, we have been unsuccessful in incorporating ^{18}O into **4** by $H_2{}^{18}O$ exchange.40 Furthermore, we were unable to obtain good resonance Raman spectra in attempts to obtain ^{18}O-labeled **4** with $H_2{}^{18}O_2$.

Interestingly, bands at 1003 and 1150 cm^{-1} were also observed in the resonance Raman spectrum of **4**, but these features were found not to be resonance enhanced (Figure 5). Such vibrations are characteristic of metal-bound sulfinate S-O vibrations ($\nu_s(SO_2)$ = ~ 950 – 1050 cm^{-1}, $\nu_{as}(SO_2)$ = ~1100 – 1200 cm^{-1}).41 Similar features were observed at 1003 and 1140 cm^{-1} in the infrared spectrum of **3** (Supporting Information, Figure S7), demonstrating that a sulfinate moiety is also present in **3**. Given the good agreement between the vibrational data obtained for **3** and **4**, we conclude that the sulfur atom is the lone oxidation site when two equivalents of peracid are reacted with **1**, generating initially iron(II)-sulfinate **3**; the third equivalent of peracid then yields oxoiron(IV)-sulfinate **4**.

3.1.5 Characterization of [Fe^{II}(TMC)(O_2SPh)](O_2SPh), 6—In order to gain a greater understanding of the structural nature of intermediates **3** and **4** we synthesized a non-appended iron-sulfinate complex. The reaction of TMC with $FeCl_2$ with subsequent addition of sodium benzenesulfinate yielded quantitatively the iron(II)-sulfinate complex [Fe^{II}(TMC)(O_2SPh)](O_2SPh) (**6**), which acts as an ideal structural mimic of **3**. Crystals of **6** suitable for X-ray diffraction analysis were attained from CH_2Cl_2/Et_2O. The structure obtained contains one benzenesulfinate bound apically through an oxygen atom to the iron(II) center (Figure 6). The observed bond distances in **6** correlate well with other iron(II)-sulfinate species showing comparable Fe–O and Fe–S distances to those reported in the literature (Fe–O = 1.9–2.0 Å, Fe–S = 3.1 – 3.3 Å, Table 3).42 FTIR showed peaks at 1001 and 1152 cm^{-1} for **6** that compare favorably with those obtained for complexes **3** and **4** (Figure S8, Supporting Information). Furthermore, the Mössbauer parameters for **6** correlate well with those obtained for **3** (ΔE_Q = 3.92 mm/s, δ = 1.13 mm/s, see Table 2, and Figure S9 Supporting Information).

3.1.6 X-ray absorption spectroscopy—XANES analysis showed that **1, 3** and **6** possess relatively similar first inflection points for the Fe K-edge of 7122.4 eV, 7123.0 eV and 7123.1 eV, respectively (Table 2), all of which are consistent with an iron(II) oxidation state. The slightly higher edge energies for **3** and **6** may reflect a slightly higher effective nuclear charge on the iron center relative to **1**, as would be expected when comparing a highly basic thiolate (**1**) to a relative weak sulfinate (**3** and **6**) axial ligand. In contrast the Fe K-edge of **4** is considerably blue-shifted, with a first inflection point of 7125.7 eV, consistent with two-electron oxidation of the iron center from iron(II) in **1** and **3** to iron(IV) in **4**. The edge energy of **4** is similar to the value of 7125.1 eV previously reported for **2**19 and is consistent with the values reported previously for other oxoiron(IV) complexes with the TMC ligand.21(d)

The pre-edge feature of **1** shows clear evidence for two peaks with peak maxima at 7112.5 eV and 7114.4 eV, having respective areas of 13.6 and 3.6 units (Figure 7). Complex **6** displays pre-edge features similar to **1**, with two peaks observed at 7112.4 eV and 7114.3 eV, although they are of lower intensity than those of **1**. Earlier XANES studies of five-coordinate square pyramidal high-spin iron(II) complexes of the form [Fe^{II}(TMC)(X)] (where X = $^-$Cl, $^-$Br, $NCCH_3$, or $^-N_3$) indicated that these complexes exhibited two pre-edge peaks split by 1.8 – 2.0 eV, consistent with our observations for **1**, and **6**.43 On the other hand, the pre-edge feature of **3** can be fit to a single Gaussian peak at 7112.6 eV with a normalized pre-edge area of *ca.* 13.4 units.44 Complex **4** exhibits similar pre-edge peak properties to other non-heme oxoiron(IV) complexes, with a single peak centered at 7114.1 eV having a weighted peak area of 31.0 units. In contrast, **2** exhibits a smaller pre-edge area

of 20.0 units, likely as a result of the highly basic axial thiolate donor. We may therefore conclude that XANES analysis supports our earlier conclusions that **4** contains an oxoiron(IV) unit with a greater distortion of electronic symmetry relative to that of **2** as a result of a weaker axial donor.

We next turned to EXAFS analysis to obtain metrical details of the iron coordination environment in each of these complexes. The unfiltered $k^3\chi(k)$ EXAFS data and the corresponding Fourier transforms for **1, 3, 4**, and **6** are presented in Figure 8, along with representative best fits. Complex **1** exhibits a set of EXAFS oscillations with a largely unchanged amplitude to $k = 15$ Å^{-1}, and a relatively simple r'-space spectrum containing an intense primary peak at r' ~ 1.8 Å and relatively weak peaks at higher r'. Both **3** and **6** exhibit $k^3\chi(k)$ EXAFS spectra that are similar to one another and very different from those of **1**. Most notably, the amplitudes of the EXAFS oscillations for **3** and **6** are considerably smaller, and the r'-space spectra exhibit a clear set of distinct peaks, relative to observations for **1**. The high similarity between **3** and **6** adds weight to our hypothesis that **3** contains an O-bound Fe-sulfinate moiety. Finally, **4** exhibits $k^3\chi(k)$ EXAFS in which the EXAFS oscillations are considerably attenuated for $k > 10$ Å^{-1}, as well as a relatively simple r'-space spectrum similar to that of other [Fe^{IV}(O)(TMC)(X)] species in which the primary peak has shifted to r' ~ 1.6 Å.21(d) The latter observation is consistent with a shortening of bond lengths in the first coordination sphere upon oxidation of the iron(II) center to iron(IV).

Table 4 lists a limited set of EXAFS fits for each of **1, 3, 4**, and **6**, with the best fits for each species given in bold italics (see Tables S2 – S5, Figures S3 – S6, and accompanying text in the Supporting Information for full details of the EXAFS analysis). The primary coordination sphere of **1** can be modeled with 4 N/O scatterers at 2.19 Å and 1 sulfur scatterer at 2.29 Å, parameters consistent with the structure derived from X-ray crystallography.25 The outer shell features require multiple Fe•••C shells at 2.99 Å, 3.16 Å, and 3.54 Å in order to obtain an accurate fit (Table 4, Fit 1–5), all of which can be accounted for in the crystal structure of **1**. The improvement in F over a fit with a single Fe•••C shell at 3.07 Å indicates that this convoluted fit is justified, despite the additional complexity imparted by the multiple shells of carbon scatterers.

The EXAFS analysis of **3** indicates that there are structural differences between **3** and its precursor **1**, as might be expected from their significantly different $k^3\chi(k)$ EXAFS and r'-space spectra. The first coordination sphere can be accounted for with two shells of 3 Fe–N scatterers at 2.19 Å and a single Fe– O scatterer at 1.95 Å, in line with the structure proposed for **3** in Scheme 2. Although the number of scatterers in the 2.19-Å shell is underestimated in our best fit (Table 4, Fit 3–6), our fit results are acceptable, given the 30% uncertainty typically associated with coordination number determinations by EXAFS.45 The EXAFS features of **3** beyond the first coordination sphere are best simulated by a shell of 4 Fe•••C at 2.97 Å and a single Fe•••S interaction at 3.27 Å (Table 4, Fit 3–6). Importantly, it was not possible to introduce the Fe–S distance of 2.3 Å seen in **1** and obtain meaningful fits. Given the short Fe–O and the long Fe•••S distances, we assign the O and S shells respectively to oxygen and sulfur atoms arising from an O-bound sulfinate moiety. This assignment is further corroborated by the results obtained for **6**, where a reliable analysis was obtained with 1 Fe–O at 1.95 Å, 4 Fe–N/O at 2.18 Å, 4 Fe•••C at 2.99 Å and 1 Fe•••S at 3.28 Å (Table 4, Fit 5-4). We also note that modeling the outer-shell features of **6** with two shells of Fe•••C scatterers afforded a considerably poorer fit to the data (Table 4, Fit 5–5), lending further support to our contention that the feature at r' = 2.9 Å is associated with a sulfur scatterer. There is a discrepancy that we are unable to rationalize in the Fe–O and Fe•••S bond distances obtained for **6** using EXAFS relative to those from the crystal structure of **6** (Table 3).

Finally, the $k^3\chi(k)$ EXAFS data for **4** is best fit with the following set of parameters: 0.8 Fe=O at 1.64 Å, 5 Fe–N at 2.06 Å, and 4 Fe•••C at 2.96 Å (Table 4, Fit 4–5). The Fe=O distance of 1.64 Å is typical of values found for other [Fe^{IV}(O)(TMC)(X)] complexes (the coordination number for the 1.64-Å shell was fixed at 0.8 to account for the observation that the EXAFS sample was found by UV/Vis spectroscopy to contain 80% **4**).21(d) The 2.06-Å shell consists mainly of the TMC nitrogen donors, and the observed contraction in distance by more than 0.1 Å in **4** relative to those in **1, 3**, and **6** is consistent with the increase in oxidation state from iron(II) to iron(IV). Splitting the 2.06-Å shell to include an Fe– O scatterer at a shorter distance that could be associated with an oxygen-bound sulfinate afforded generally poorer fits as defined by the magnitude of F, and inclusion of this shell could therefore not be justified (Table S4, Supporting Information). This is the case as well in the EXAFS analyses of other [Fe^{IV}(O)(TMC)(X)] complexes except for **2**.21(d) Likewise, the available EXAFS data for **4** does not provide evidence for an Fe•••S interaction at any chemically reasonable distance. Indeed, even the addition of an Fe•••C shell at 2.96 Å to the fit leads to very modest improvements in fit quality, suggesting that scatterers other than the primary Fe–N and Fe=O shells contribute only minimally to the observed EXAFS. Consequently, EXAFS does provide direct structural evidence for the Fe=O unit in **4**, corroborating results from vibrational spectroscopy (*vide supra*), but not for a sulfur-derived species bound to the iron(IV) center *trans* to the oxo moiety.

3.1.7 Reactivity studies with 4—The reactivity of **4** towards triphenylphosphine (PPh_3) and 9,10-dihydroanthracene (DHA) was investigated for comparison with **2** and [Fe^{IV}(O)(TMC)($NCCH_3$)]$^{2+}$ (Table 5). Oxo transfer to triphenylphosphine was found to be quantitative, while anthracene was obtained in 40% yield, corresponding to the consumption of 80% of **4**. The obtained second order rate constant (k_2) values show that **4** is comparable to [Fe^{IV}(O)(TMC)($NCCH_3$)]$^{2+}$ in oxo-transfer reactivity and to **2** in H-atom abstraction reactivity.21(c) Interpretation of these results within the context of the trends observed for a series of four [Fe^{IV}(O)(TMC)(X)] complexes46 is not straightforward. Consistent with the spectroscopic data obtained for **4** described above, the PPh_3 oxidation rates suggest that **4** has an axial ligand with a basicity that affords an Fe=O unit of comparable electrophilicity to that of [Fe^{IV}(O)(TMC)($NCCH_3$)]$^{2+}$. However, the observation that the DHA oxidation rate found for **4** is a factor of 20 faster than that of [Fe^{IV}(O)(TMC)($NCCH_3$)]$^{2+}$ and comparable to that of **2** is not consistent with this conclusion. This suggests that our understanding of what factors control the reactivity of an Fe^{IV}=O unit in H-atom abstraction requires further refinement. It is also possible that the presence of protons from *m*-CBA may affect the rate of H-atom abstraction. Given this complexity, the DHA oxidation rate may not be reliable as an indicator of the axial-ligand donor in an [Fe^{IV}(O)(TMC)(X)] complex.

3.1.8 Summary—Our accumulated observations lead us to conclude that the addition of up to two equivalents of peracid to **1** results in the oxidation of the bound thiolate to a sulfinate in **3**, without evidence for an intervening sulfenate species. The addition of another (third) equivalent of peracid (Scheme 2) results in the conversion of the formed O-bound iron(II)-sulfinate complex to the corresponding oxoiron(IV)-sulfinate (**4**, $\nu_{Fe=O}$ = 831 cm^{-1}, Fe–O = 1.64 Å) species with properties similar to a family of [Fe^{IV}(O)(TMC)(X)] complexes reported previously.21(d) The combined spectroscopic evidence indicates the presence of a weak field axial donor in **4**, most likely the sulfinate moiety identified by vibrational spectroscopy (ν_s(SO2) = 1003 cm^{-1}, ν_{as}(SO2) = 1150 cm^{-1}).

3.2 Elucidating the mechanism of sulfur oxidation

In metal-thiolate complexes sulfur oxidation may occur either as a result of direct reaction between the bound thiolate and oxidant, or as a result of metal-mediated oxidation. Darensbourg and co-workers have carried out a number of investigations into sulfur

oxidation in nickel(II)-dithiolate complexes,47 in which both sulfur-bound sulfenate and sulfinates were generated, depending on the oxidant used.48 Sulfur oxidation was proposed to result from nucleophilic attack by the bound thiolate on an electrophilic oxygen atom in dioxygen or H_2O_2. *No evidence for metal-based oxidants was found*. In attempting to mimic CDO, Goldberg presented evidence for metal-mediated oxygenation by O_2 of an iron(II)-thiolate complex yielding a iron(II)-sulfonate complex.16 In studies on iron and cobalt NHase mimics a number of metal-sulfenate, -sulfinate and -sulfonate complexes have been synthesized by reaction between the metal(III)-thiolate complex and various oxidants (e.g. dioxygen, H_2O_2, oxiranes).12–18 Grapperhaus observed that in the reaction between an S = 1/2 iron(III)-dithiolate complex and dioxygen an iron(III)-disulfonate was formed.15 Conversely, the S = 5/2 analogue yielded disulfide and non-ligated iron products. In one mass spectrometry study, the reaction of an iron(III)-thiolate complex and dioxygen resulted in the initial formation of an iron(III)-sulfenate, which over time was converted to iron(III)-sulfinate.49 The reaction between a heme iron(III)-thiolate model compound and one equivalent of *m*-CPBA yielded an oxoiron(IV) Compound I mimic.17(c) The same reaction carried out with excess *m*-CPBA yielded the S-oxidized iron(III)-sulfonate product. Unfortunately, not much insight was reported as to the mechanism of sulfur oxidation in any of these iron and cobalt model complexes. Given the dearth of mechanistic information, we have further investigated the conversion of **1** to **3** to elucidate whether S-oxidation was purely an organic transformation or was metal-mediated.

To gain a better understanding of the susceptibility of the thiolate moiety in **1** and **2** to S-oxidation by nucleophilic attack of the sulfur on an electrophilic oxygen atom, we investigated their reactivity towards oxo-atom transfer reagents other than *m*-CPBA. As previously reported,19 addition of 6 equivalents of H_2O_2 with no added acid or base to a methanolic solution of **1** at - 40 °C resulted in the formation of **2** in 45% yield in approximately 10 minutes, as determined by electronic absorption and Mössbauer spectroscopies. Mössbauer analysis showed that neither **3** nor **4** was detected in significant amounts in these samples. In contrast, the same reaction carried out in the presence of excess benzoic acid (10 equiv. $PhCO_2H$, chosen to mimic *m*-CBA) resulted in the formation of **4** (instead of **2**) over a period of 2 hours (60% yield), as evidenced by the formation of near-IR electronic absorption features (λ_{max} = 830 and 990 nm) and the observation of a mass peak (m/z = 405.2) consistent with **4**. The observed differences in reactivity, in the absence and presence of *acid*, show that the availability of H^+ controls whether **2** or **4** form upon exposure of **1** to H_2O_2. This observation parallels observations made with *m*-CPBA in the presence and absence of *base*.

We investigated the susceptibility of **1** to oxidation by iodosylbenzene and oxoiron(IV) complexes to get a greater understanding of the nucleophilicity of the bound thiolate ligand. When **1** was exposed at −20 °C to either iodosylbenzene, $[Fe^{IV}(O)(TMC)(NCCH_3)]^{2+}$, $[Fe^{IV}(O)(N4Py)]^{2+}$ or **2**, no sulfur oxidation products were observed by ESI-MS. However, the reaction between **1** and iodosylbenzene in the presence of 10 equiv. $PhCO_2H$ showed evidence for the formation of **3** and iron(III)-thiolate byproducts. Furthermore, the self-decay of **2** yielded the same iron(III)-thiolate species, and not the sulfur oxidized product **3**.19 It must also be noted that neither **1** nor **2** reacted with dioxygen. These results demonstrate that the thiolate ligands of **1** and **2** are unlikely to undergo S-oxidation by nucleophilic sulfur attack on an electrophilic oxygen atom, unless an excess of H^+ is present.

Further insight into the reaction chemistry between a metal(II)-TMCS complex and *m*-CPBA was obtained with the redox-inactive complex $[Zn^{II}(TMCS)]PF_6$ (**7**). Exposure of a 1 mM methanolic solution of **7** to two equivalents of m-CPBA at −20 °C (mimicking the conversion of **1** to **3**) resulted in the formation of sulfinate complex $[Zn^{II}(TMCSO_2)]^+$ within 60 s. ESI-MS showed the incorporation of two oxygen atoms (Figure 9), while FTIR

showed peaks at 1001 and 1145 cm^{-1} typical of metal-bound sulfinate (Supporting Information, Figure S10). The FTIR results compare favorably with those obtained by IR and rR for compounds **3** and **4**, respectively. Importantly, no S-oxidized products were observed in the presence of excess base (KO^tBu). The conclusion can therefore be drawn that direct S-oxidation by *m*-CPBA can occur in the conversion of **1** to **3**.

The reaction of **1** with peracid in the absence of base results in preferential sulfur oxidation over iron oxidation (Scheme 2), while excess strong base (KO^tBu) is required for the generation of **2**. The strong base may act in one of two ways: a) by deprotonation of *m*-CPBA to enhance binding of its conjugate base to the vacant site on the iron(II) center in **1**; *OR* b) by neutralizing H^+ formed in the reaction that may promote sulfur oxidation. That base is not required for the formation of **2** from less acidic H_2O_2 suggests that deprotonation of H_2O_2 is not necessary, showing that factor (a) does not play a significant role in directing the formation of **2**. To gain a greater understanding of the mechanism of sulfur oxidation we investigated the effect of adding H^+ to both **1** and **2**.

The introduction of 10 equivalents $PhCO_2H$ (pK_a = 4.2) or trifluoroacetic acid (TFA, pK_a = 0.5) to **1** in methanol at −20 °C did not affect the UV-vis spectrum of **1**. The intensity of the λ_{max} = 320 nm feature belonging to **1** was maintained over a period of twenty minutes in the presence of benzoic acid, and no new absorption features were observed. On the other hand, addition of 6 equivalents of H^+ (to neutralize the 6 eq KO^tBu present, $PhCO_2H$, TFA or pyridinium triflate are all suitable proton sources) to a solution of **2** at −20 °C resulted in the rapid decomposition of **2**, as indicated by the disappearance of the charge transfer bands in the visible region characteristic of **2** (λ_{max} = 460 and 570 nm) and a decrease in intensity of the near-IR features (Figure 10). Mössbauer spectroscopy showed the *complete* loss of **2** and the appearance of two components: **3** (47%, δ = 1.01 mm/s, ΔE_Q = 3.77 mm/s), and an iron(IV) species (**5**, 38%, δ = 0.16 mm/s, ΔE_Q = 1.15 mm/s, Figure 11). For **5** the isomer shift is indicative of an [Fe^{IV} (O)(TMC)(X)] center21(d) and its quadrupole splitting is suggestive of an axial donor considerably less basic than the thiolate ligand in **2** and somewhat more basic than that of **4**.21(d) We propose that this species is the conjugate acid of **2**, where the thiolate ligand is protonated and could be displaced by the solvent MeOH or benzoate, formed as a result of $PhCO_2H$ neutralization of KO^tBu.

These results show that **2** can be converted to **3**, implicating a metal-based oxidant in sulfur oxidation. The yield of S-oxidized product **3** (47%), accounts for approximately 100% of O-atoms derived from starting material **2**. We believe that **5** (yield 38%) retains an O-atom from **2**, thus giving an overall oxygen atom stoichiometry of 140%. We suspect that the extra oxygen atoms are derived from excess peracid present in solution in the Mössbauer experiment (1.2 equivalents of *m*-CPBA were added to **1** to generate **2** in 75% yield). Alternatively, dioxygen may play a role in converting the free thiol of **5** or a transient sulfenate to sulfinate **3**, thus accounting for the higher than expected oxygen atom yield.

These results show that the iron(II)-thiolate bond in **1** is stable to acidic conditions. On the other hand, the iron(IV)-thiolate bond in **2** appears more susceptible to protonation by $PhCO_2H$, as indicated by the disappearance of the visible features corresponding to thiolate-to-iron CT transitions (Figure 10). The greater susceptibility of the iron(IV)-thiolate bond to protonation compared to the iron(II)-thiolate may seem counterintuitive at first glance, because the iron(IV)-thiolate bond may be expected to be the stronger of the two. However, the oxo group *trans* to the thiolate ligand in **2** could exert a labilizing influence. Indeed the structural analysis of **1**25 and **2**19 shows that the Fe–S bond increases marginally in length upon going from **1** to **2** (2.30 *vs* 2.33 Å, respectively), despite the increase in iron oxidation state from +2 to +4 as well as a change in spin-state from S = 2 to S = 1. Both of these factors are expected to shorten the Fe–S bond in **2** but apparently do not, presumably

because of the *trans* influence of the oxo ligand. Thus the weaker than expected iron(IV)-thiolate interaction allows the thiolate to be protonated by $PhCO_2H$ and become displaced from the iron(IV) center by MeOH, resulting in the species we assign as **5**.

In the reaction between **2** and H^+ to yield **3** and **5**, the loss of the thiolate ligand from **2** should make **5** a much better oxygen atom transfer reagent than **2**, which has been shown to be very sluggish in such reactions, because the highly basic thiolate has been replaced by a less basic ligand (Scheme 3).21(c) At the same time the hypothesized free thiol becomes a target for S-oxidation. Because we have found no evidence to date for the formation of an oxoiron(IV) complex with a sulfenate tail, such a species must be oxidized more rapidly than **5** to be consistent with our observations. The product of the second cycle of oxidation would be **4**, which in turn is converted to **3** upon transfer of its oxo atom to another molecule of **5** (for complete Scheme 3 see Scheme S11 in Supporting Information). Thus, in the conversion of **1** to **3**, a plausible reaction mechanism is that *m*-CPBA reacts with the iron(II) center of **1** to generate **5**, which in turn transfers the oxygen atom to the thiol of a second molecule of **5** (Scheme 3, pathway A).50 Indeed, a small amount of **5** *was* observed to form in the conversion of **1** to **3** (Figures 1, 3(C), and 4), (Mössbauer, 8% yield), thereby implicating **2** as a likely intermediate. However, direct sulfur oxidation by *m*-CPBA of **1** yielding **3** is also a plausible outcome as demonstrated by the reaction between **7** and *m*-CPBA (Scheme 3, pathway B).

Investigations into IPNS using substrate analogs have shown that the thiol sulfur can be oxidized to a sulfenic acid, presumably via the putative oxoiron(IV) oxidant formed in the catalytic cycle.6 The mechanism of conversion of cysteine to cysteinesulfinic acid by CDO is currently hypothesized to be effected either by a low-valent iron superoxide moiety or a high valent iron-oxo moiety as a basis for the mechanism of sulfur oxidation.5(a) Recent X-ray crystallographic work showed evidence for an intermediate iron(II)-persulfenate species, leading the authors to propose the catalytic cycle involves no high valent iron intermediates. 5(d) However, elsewhere oxoiron(IV) species have been hypothesized as likely oxidizing moieties in CDO.5(a,c) Little is know about the mechanism of S-oxidation in the post-translational formation of sulfenate and sulfinate functionalities on active site cysteine residues in the maturation of Fe-NHase.8,15 Furthermore, the role of metal-based oxidants and in particular oxoiron(IV) species in this transformation has not been investigated to date. Our observations compellingly show that indeed under the correct conditions an oxoiron(IV) moiety can reliably generate a sulfinate in high yields.

4. Conclusions

Drastically different reactivities between an iron(II)-thiolate complex and peracid were observed depending on the availability of protons. Under highly basic conditions iron(IV) thiolate species **2** is formed,19 but under slightly acidic conditions (reported herein) iron(II)-sulfinate complex **3** is obtained instead. We have investigated the structural and electronic properties of the formed iron(II)-sulfinate, proving its existence, and have also shown that it will readily convert to oxoiron(IV)-sulfinate **4**, whose properties have also been thoroughly investigated. The apparent preferential sulfur versus iron oxidation, depending on the availability of protons, is in fact quite complex. Investigations into $[Zn^{II}(TMCS)]^+$ have shown that direct S-oxidation of a metal-bound thiolate can occur, showing that the conversion of **1** to **3** does not necessarily require a redox-active metal center. Conversely, we have observed metal-oxidized intermediates ($[Fe^{IV}(O)(TMCSH)]$) in the conversion of **1** to **3**. Furthermore, we have demonstrated that oxoiron(IV)-thiolate **2** will readily convert to **3** in the presence of H^+, suggesting that metal-mediated S-oxidation is also a credible pathway in the conversion of **1** to **3**. These results demonstrate that oxoiron(IV)

intermediates are plausible as S-oxidants in the formation of oxygenated thiolate moieties found in the chemistry of CDO, NHase, and IPNS.

Supplementary Material

Refer to Web version on PubMed Central for supplementary material.

Acknowledgments

This publication was made possible by funding from the US National Institutes of Health (grants GM-33162 to L. Q. and EB-001475 to E. M., post-doctoral fellowship GM-087895 to A. McD., and pre-doctoral traineeship GM-08700 to E. R. F.), NRF of Korea through CRI and WCU (R31-2008-000-10010-1) programs (W. N.), and the US National Science Foundation (J. A. H., CHE-0615479). The authors would like to thank Dr. Victor G. Young, Jr. of the University of Minnesota X-Ray Crystallographic Laboratory for the solution of the X-ray crystal structure of compound **6**. XAS data were collected on beamline X9B at the National Synchrotron Radiation Lightsource (NSLS), Brookhaven National Laboratory, and on beamline 7-3 at the Stanford Synchrotron Radiation Lightsource (SSRL). NSLS is supported by the U.S. Department of Energy, Office of Science, Office of Basic Energy Sciences, under Contract No. DE-AC02-98CH10886. SSRL is a national user facility operated by Stanford University on behalf of the U.S. Department of Energy, Office of Basic Energy Sciences. The SSRL Structural Molecular Biology Program is supported by the Department of Energy, Office of Biological and Environmental Research, and by the National Institutes of Health, National Center for Research Resources, Biomedical Technology Program. We thank Drs. Nebjosa Marinkovic (NSLS X9B), Allyson Aranda (SSRL 7-3), and Matthew Latimer (SSRL 7-3) for excellent technical support of our XAS experiments.

References

1. (a) Groves JT. J. Inorg. Biochem. 2006; 100:434–447. [PubMed: 16516297] (b) Schlichting I, Berendzen J, Chu K, Stock AM, Maves SA, Benson DE, Sweet RM, Ringe D, Petsko GA, Sligar SG. Science. 2000; 287:1615–1622. [PubMed: 10698731]
2. (a) Auclair K, Moënne-Loccoz P, Ortiz de Montellano PR. J. Am. Chem. Soc. 2001; 123:4877–4885. [PubMed: 11457314] (b) Ogliaro F, de Visser SP, Shaik SJ. Inorg. Biochem. 2002; 91:554–567.
3. (a) Mathé C, Weill CO, Mattioli TA, Berthmoieu C, Houée-Levin C, Tremey E, Nivière V. J. Biol. Chem. 2007; 282:22207–22216. [PubMed: 17545670] (b) Kovacs JA, Brines LM. Acc. Chem. Res. 2007; 40:501–509. [PubMed: 17536780]
4. McCoy JG, Bailey LJ, Bitto E, Bingman CA, Aceti DJ, Fox BG, Phillips GN Jr. Proc. Nat. Acad. Sci. 2006; 103:3084–3089. [PubMed: 16492780]
5. (a) Joseph CA, Moroney MJ. Chem. Commun. 2007:3338–3349.(b) Aluri S, de Visser SP. J. Am. Chem. Soc. 2007; 129:14846–14847. [PubMed: 17994747] (c) We S, Wu X, Wei L, Tang D, Sun P, Bartlam M, Rao Z. J. Biol. Chem. 2007; 282:3391–3402. [PubMed: 17135237] (d) Simmons CR, Krishnamoorthy K, Granett SL, Shuller DJ, Dominy JE Jr, Begley TP, Stipanuk MH, Karplus PA. Biochemistry. 2008; 47:11390–11392. [PubMed: 18847220]
6. (a) Roach PL, Clifton IJ, Hensgens CMH, Shibata N, Schofield CJ, Hajdu J, Baldwin JE. Nature. 1997; 387:827–830. [PubMed: 9194566] (b) Burzlaff NI, Rutledge PJ, Clifton IJ, Hensgens CMH, Pickford M, Adlington RM, Roach PL, Baldwin JE. Nature. 1999; 401:721–724. [PubMed: 10537113]
7. Ge W, Clifton IJ, Stok JE, Adlington RM, Baldwin JE, Rutledge PJ. J. Am. Chem. Soc. 2008; 130:10096–10102. [PubMed: 18620394]
8. (a) Nagashima S, Nakasako M, Dohmae N, Tsujimura M, Takio K, Odaka M, Yohda M, Kamiya N, Endo I. Nat. Struct. Biol. 1998; 5:347–351. [PubMed: 9586994] (b) Endo I, Nojiri M, Tsujimura M, Nakasako M, Nagashima S, Yohda M, Odaka M. J. Inorg. Biochem. 2001; 83:247–253. [PubMed: 11293544]
9. (a) Murakami T, Nojiri M, Nakayama H, Odaka M, Yohda M, Dohmae N, Takio K, Nagamune T, Endo I. Protein Science. 2000; 9:1024–1030. [PubMed: 10850812] (b) Stevens JM, Belghazi M, Jaouen M, Bonnet D, Schmitter J-M, Mansuy D, Sari M-A, Artaud I. J. Mass. Spec. 2003; 38:955–961.
10. Kovacs JA. Chem. Rev. 2004; 104:825–848. [PubMed: 14871143]

11. (a) Kitagawa T, Dey A, Lugo-Mas P, Benedict JB, Kaminsky W, Solomon EI, Kovacs JA. J. Am. Chem. Soc. 2006; 128:14448–14449. [PubMed: 17090014] (b) Krishnamurthy D, Kasper GD, Namuswe F, Kerber WD, Narducci Sarjeant AA, Moënne-Loccoz P, Goldberg DP. J. Am. Chem. Soc. 2006; 128:14222–14223. [PubMed: 17076472] (c) Bukowski MR, Halfen HL, van den Berg TA, Halfen JA, Que L Jr. Angew. Chem. Int. Ed. 2005; 44:584–587.(d) Namuswe F, Kasper GD, Narducci Sarjeant AA, Hayashi T, Krest CM, Green MT, Moenne-Loccoz P, Goldberg DP. J. Am. Chem. Soc. 2008; 130:14189–14200. [PubMed: 18837497] (e) Jiang Y, Telser J, Goldberg DP. Chem. Commun. 2009; 44:6828–6830.
12. Galardon E, Giorgi M, Artaud I. Chem. Commun. 2004:286–287.
13. (a) Rat M, de Sousa RA, Vaissermann J, Leduc P, Mansuy D, Artaud I. J. Inorg. Biochem. 2001; 84:207–213. [PubMed: 11374583] (b) Bourles E, de Sousa RA, Galardon E, Giorgi M, Artaud I. Angew. Chem. Int. Ed. 2005; 44:6162–6165.
14. (a) Lugo-Mas P, Taylor W, Schweitzer D, Theisen RM, Xu L, Shearer J, Swartz RD, Gleaves MC, DiPasquale A, Kaminsky W, Kovacs JA. Inorg. Chem. 2008; 47:11228–11236. [PubMed: 18989922] (b) Lugo-Mas P, Dey A, Xu L, Davin SD, Benedict J, Kaminsky W, Hodgson KO, Hedman B, Solomon EI, Kovacs JA. J. Am. Chem. Soc. 2006; 128:11211–11221. [PubMed: 16925440] (c) Kung I, Schweitzer D, Shearer J, Taylor WD, Jackson HL, Lovell S, Kovacs JA. J. Am. Chem. Soc. 2000; 122:8299–8300.
15. O'Toole MG, Kreso M, Kozlowski PM, Mashuta MS, Grapperhaus CA. J. Biol. Inorg. Chem. 2008; 13:1219–1230. [PubMed: 18633652]
16. Jiang Y, Widger LR, Kasper GD, Siegler MA, Goldberg DP. J. Am. Chem. Soc. 2010 ASAP, DOI: 10.1021/ja105591q.
17. (a) Kozuch S, Leifels T, Meyer D, Sbaragli L, Shaik S, Woggon W-D. Synlett. 2005; 4:675–684. (b) Meyer D, Leifels T, Sbaragli L, Woggon W-D. Biochem. Biophys. Res. Commun. 2005; 338:372–377. [PubMed: 16111653] (c) Hessenauer-Ilicheva N, Franke A, Wolak M, Higuchi T, van Eldik R. Chem. Eur. J. 2009; 15:12447–12459. [PubMed: 19806618]
18. Noveron JC, Olmstead MM, Mascharak PK. J. Am. Chem. Soc. 2001; 123:3247–3259. [PubMed: 11457060]
19. Bukowski MR, Koehntop KD, Stubna A, Bominaar EL, Halfen JA, Münck E, Nam W, Que L Jr. Science. 2005; 310:1000–1002. [PubMed: 16254150]
20. (a) Que L Jr. Acc. Chem. Res. 2007; 40:493–500. [PubMed: 17595051] (b) Nam W. Acc. Chem. Res. 2007; 40:522–531. [PubMed: 17469792]
21. (a) Rohde J-U, In J-H, Lim MH, Brennessel WW, Bukowski MR, Stubna A, Münck E, Nam W, Que L Jr. Science. 2003; 299:1037–1039. [PubMed: 12586936] (b) Sastri C, Park MJ, Ohta T, Jackson TA, Stubna A, Seo MS, Lee J, Kim J, Kitagawa T, Münck E, Que L Jr, Nam W. J. Am. Chem. Soc. 2005; 127:12494–12495. [PubMed: 16144389] (c) Sastri C, Lee J, Oh K, Lee YJ, Lee J, Jackson TA, Ray K, Hirao H, Shin W, Halfen JA, Kim J, Que L Jr, Shaik S, Nam W. Proc. Nat. Acad. Sci. 2007; 104:19181–19186. [PubMed: 18048327] (d) Jackson TA, Rohde J-U, Seo MS, Sastri CV, DeHont R, Stubna A, Ohta T, Kitigawa T, Münck E, Nam W, Que L Jr. J. Am. Chem. Soc. 2008; 130:12394–12407. [PubMed: 18712873]
22. (a) Lim MH, Rohde J-U, Stubna A, Bukowski MR, Costas M, Ho RYN, Münck E, Nam W, Que L Jr. Proc. Nat. Acad. Sci. 2003; 100:3665–3670. [PubMed: 12644707] (b) Kaizer J, Costas M, Que L Jr. Angew. Chem. Int. Ed. 2003; 42:3671–3673.(c) Rohde J-U, Stubna A, Bominaar EL, Münck E, Nam W, Que L Jr. Inorg. Chem. 2006; 45:6435–6445. [PubMed: 16878956]
23. (a) Kaizer J, Klinker EJ, Oh NY, Rohde J-U, Song WJ, Stubna A, Kim J, Münck E, Nam W, Que L Jr. J. Am. Chem. Soc. 2004; 126:472–473. [PubMed: 14719937] (b) Klinker EJ, Kaizer J, Brennessel WW, Woodrum NL, Cramer CJ, Que L Jr. Angew. Chem. Int. Ed. 2005; 44:3690–3694.
24. Halfen JA, Young VG. Chem. Commun. 2003:894–2895.
25. Fiedler AT, Halfen HL, Halfen JA, Brunold TC. J. Am. Chem. Soc. 2005; 127:1675–1689. [PubMed: 15701002]
26. Armarego, WLF.; Perrin, DD. Purification of Laboratory Chemicals. Butterworth-Heinemann: Oxford Press; 1997.
27. SMART V5.054. Madison, WI: Bruker Analytical X-ray Systems; 2001.

28. An empirical correction for absorption anisotropy, R. Blessing. Acta Cryst. 1995; A51:33–38.
29. SAINT+ V6.45. Madison, WI: Bruker Analytical X-Ray Systems; 2003.
30. SHELXTL V6.14. Madison, WI: Bruker Analytical X-Ray Systems; 2000.
31. George, GN. EXAFSPAK; Stanford Synchrotron Radiation Lightsource. Stanford, CA: SLAC National Accelerator Laboratory; 2000.
32. Scarrow RC, Brennan BA, Cummings JG, Jin H, Duong DJ, Kindt JT, Nelson MJ. Biochemistry. 1996; 35:10078–10088. [PubMed: 8756470]
33. Rohde J-U, Torelli S, Shan X, Lim MH, Klinker EJ, Kaizer J, Chen K, Nam W, Que L Jr. J. Am. Chem. Soc. 2004; 126:16750–16761. [PubMed: 15612713]
34. Ankudinov AL, Ravel B, Rehr JJ, Conradson SD. Phys. Rev. B. 1998; 58:7565.
35. Decker A, Rohde J-U, Que L Jr, Solomon EI. J. Am. Chem. Soc. 2004; 126:5378–5379. [PubMed: 15113207]
36. ESI-MS analysis of the reaction solution once **4** had decayed showed peaks that correspond to $[Fe(III)(OMe)(TMCSO_3)]^+$. This species decays further when left to stand at room temperature to iron salts and $[2H^+ + TMCSO_3]$ according to ESI-MS.
37. Münck, E. Chap. 6. In: Que, L., Jr, editor. Physical Methods in Bioinorganic Chemistry. Sausalito, CA: University Science Books; 2000. p. 287-320.
38. Peaks corresponding to **4** are of comparable intensity to those of **3** in Figure 4C, despite evidence from Mössbauer spectroscopy that **3** is the dominant product (92%). We also saw evidence that the sulfinate species **3** and **4** were being further oxidized in the ionization chamber to sulfonate - thus producing signals corresponding to both iron(II) sulfonate, and Fe^{IV}-sulfonate.
39. See Figure 11 in ref. 21(d). Insertion of a point for **4** (pre-edge area = 31 a.u., $\nu_{Fe=O} = 831\ cm^{-1}$, $\Delta E_Q = 1.32\ mm/s^{-1}$) shows good agreement with the plot/trend observed, supporting the assignment of a weak axial donor in **4**
40. Seo MS, In J-H, Kim SO, Oh NY, Hong J, Kim J, Que L Jr, Nam W. Angew. Chem. Int. Ed. 2004; 43(18):2417–2420.
41. Vitzthum G, Lindner E. Angew. Chem. Int. Ed. 1971; 10:315–326.
42. (a) Cocolios P, Lagrange G, Guilard R, Oumous H, Lecomte C. J. Chem. Soc., Dalton Trans. 1984:567–574.(b) Heinrich L, Li Y, Vaissermann J, Chottard G, Chottard J-C. Angew. Chem. Int. Ed. 1999; 38:3526–3528.(c) Noveron JC, Olmstead MM, Mascharak PK. J. Am. Chem. Soc. 2001; 123:3247–3259. [PubMed: 11457060]
43. Westre TE, Kennepohl P, DeWitt JG, Hedman B, Hodgson KO, Solomon EI. J. Am. Chem. Soc. 1997; 119:6297–6314.
44. The lack of a second peak in **3** can be largely attributed to the lower resolution of the Si(111) crystal monochromator at NSLS X9B compared with the Si(220) crystal monochromator used at SSRL 7-3. Similar observations have been made in XAS studies of MMOH.
45. (a) Penner-Hahn JE. Coord. Chem. Rev. 1999; 190–192:1101–1123.(b) Yano J, Yachandra VK. Photosyn. Res. 2009; 102:241–254. [PubMed: 19653117]
46. Hirao H, Que L Jr, Nam W, Shaik S. Chem. Eur. J. 2008; 14:1740–1756. [PubMed: 18186094]
47. (a) Grapperhaus CA, Darensbourg MY. Acc. Chem. Res. 1998; 31:451–459.(b) Kaasjager VE, Bouwman E, Gorter S, Reedijk J, Grapperhaus CA, Reibenspies JH, Smee JJ, Darensbourg MY, Derecskei-Kovacs A, Thomson LM. Inorg. Chem. 2002; 41:1837–1844. [PubMed: 11925177] (c) Chohan BS, Maroney MJ. Inorg. Chem. 2006; 45:1906–1908. [PubMed: 16499349] (d) Moroney MJ, Choudhury SB, Bryngelson PA, Mirza SA, Sherrod MJ. Inorg. Chem. 1996; 35:1073–1076. [PubMed: 11666287] (e) Liu T, Li B, Singleton ML, Hall MB, Darensbourg MY. J. Am. Chem. Soc. 2009; 131:8296–8307. [PubMed: 19507910]
48. Buonomo RM, Font I, Maquire MJ, Reibenspies JH, Tuntulani T, Darensbourg MY. J. Am. Chem. Soc. 1995; 117:963–973.
49. Noveron JC, Olmstead MM, Mascharak PK. J. Am. Chem. Soc. 2001; 123:3247–3259. [PubMed: 11457060]
50. In contrast, Kodanko has recently shown that the reaction between an oxoiron(IV) complex $(Fe^{IV}(O)(N4Py)]^{2+}$) and the thiol containing tripeptide glutathione yields thiolatoiron(III)-N4Py and disulfide. No sulfenate, sulfinate or sulfonate products were observed. Campanali AA,

Kwiecien TD, Hryhorczuk L, Kodanko JJ. Inorg. Chem. 2010; 49:4759–4761. [PubMed: 20446674]

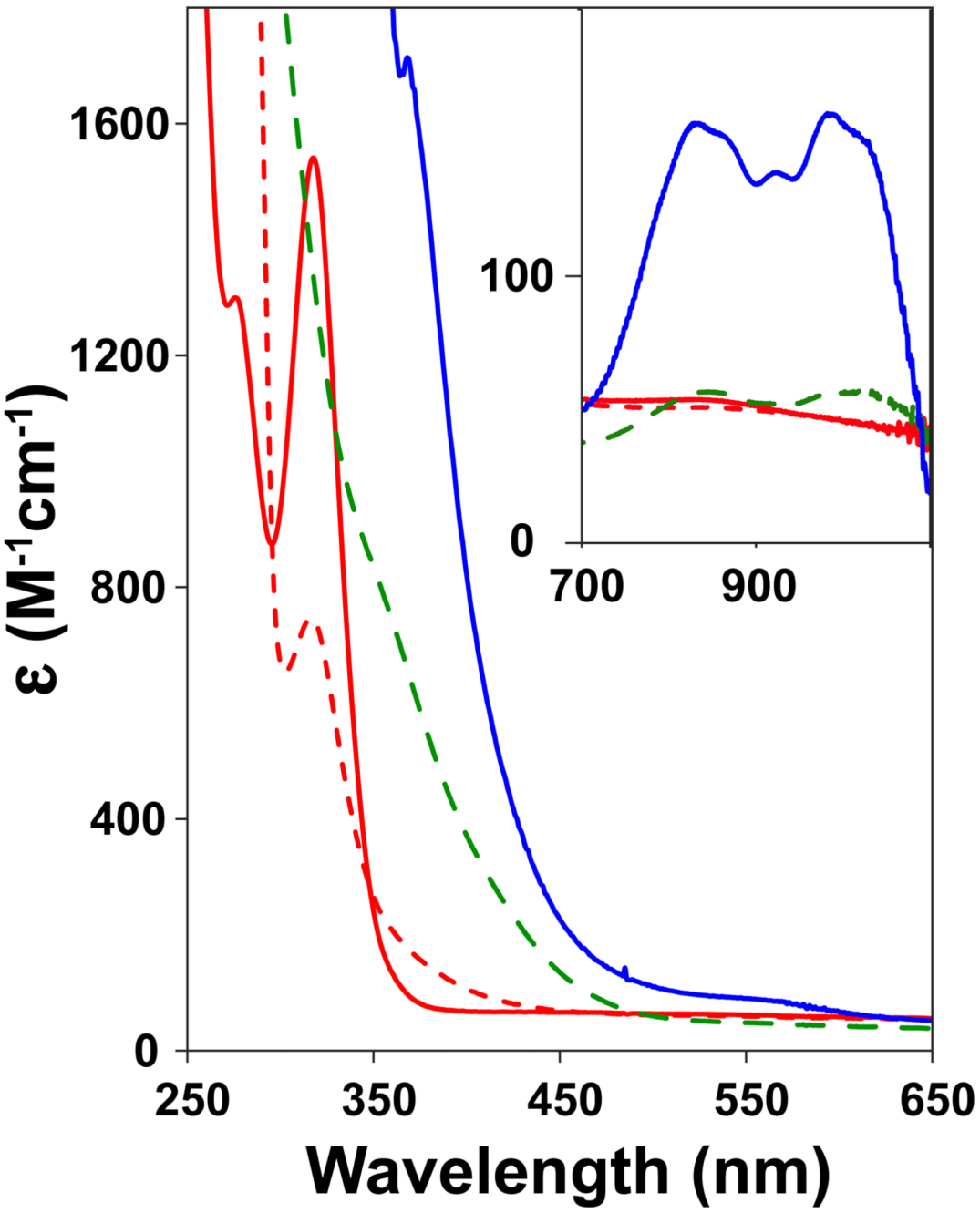

Figure 1.
UV-Vis spectral changes upon titration of **1** with *m*-CPBA in MeOH. Red solid line: 0 equiv.; red dashed line: 1 equiv.; green dashed line: 2 equiv. to form **3**; blue solid line: 3 equiv. to form **4**.

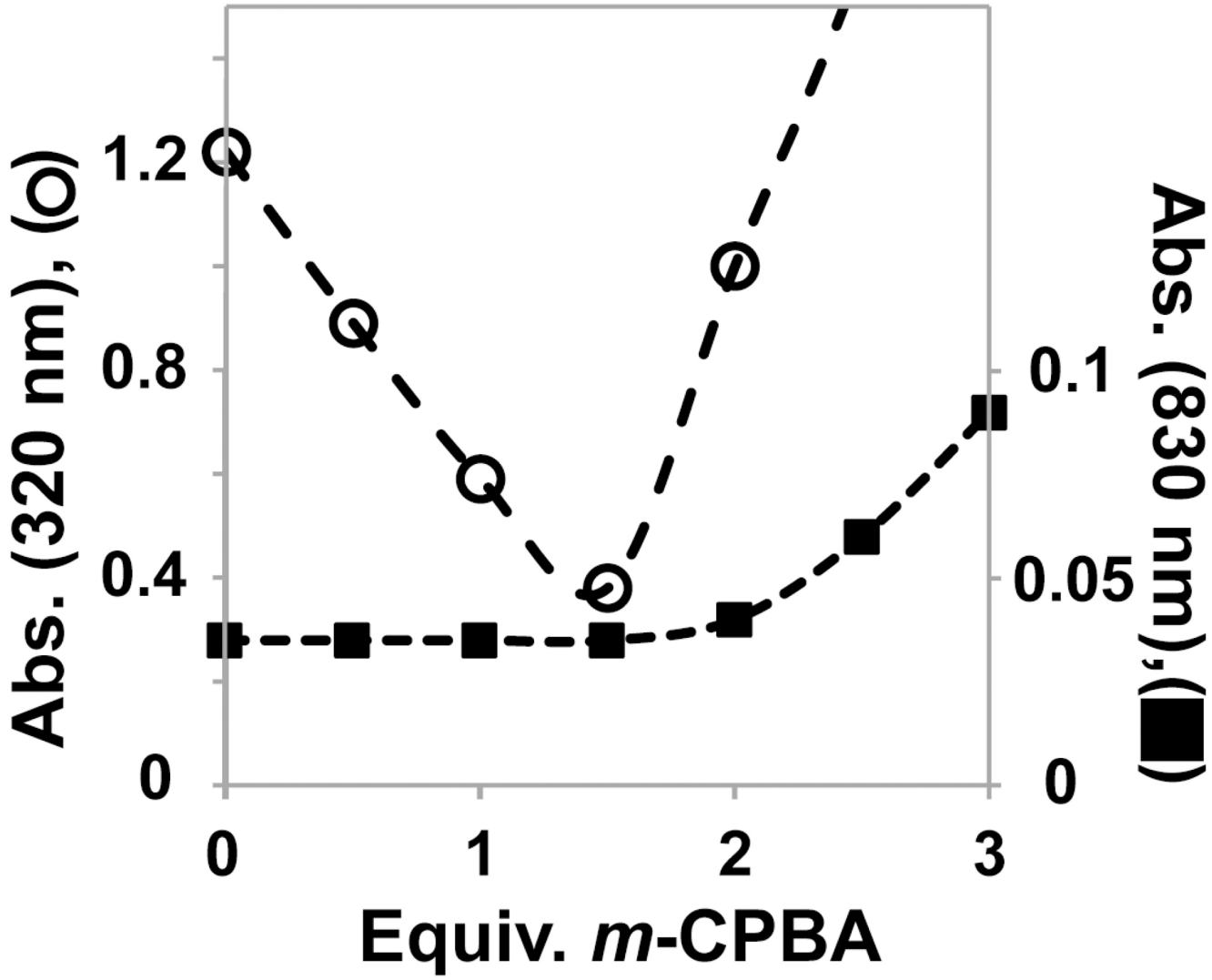

Figure 2.
Plot of titration of oxidant (*m*-CPBA) with **1** (0.85 mM) against intensity of absorption features assigned to **1** (•, λ_{max} = 320 nm, left) and **4** (■, λ_{max} = 830 nm, right).

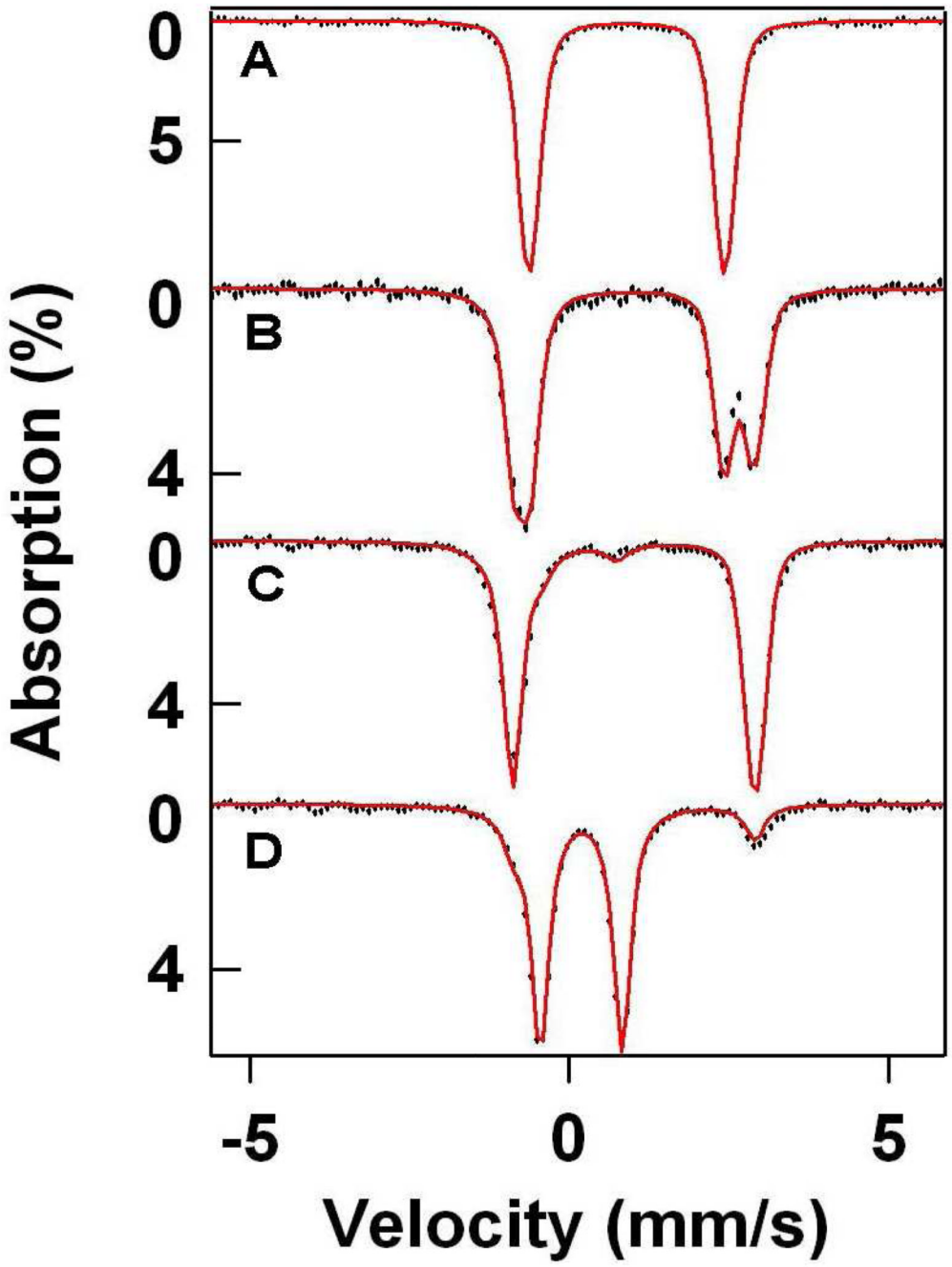

Figure 3.

The 4.2-K Mössbauer spectra of **1, 3**, and **4** recorded in zero field (1.5 mM Fe, MeOH solvent). Spectra are shown as hash-marks, while spectral simulations are shown as lines: (A) **1**; (B) **1** + 1 equiv. *m*-CPBA (50% **1**, 50% **3**); (C) **1** + 2 equiv. *m*-CPBA (92% **3**, 8% **5**); (D) **1** + 3 equiv. *m*-CPBA (86% **4**, 14% **3**)

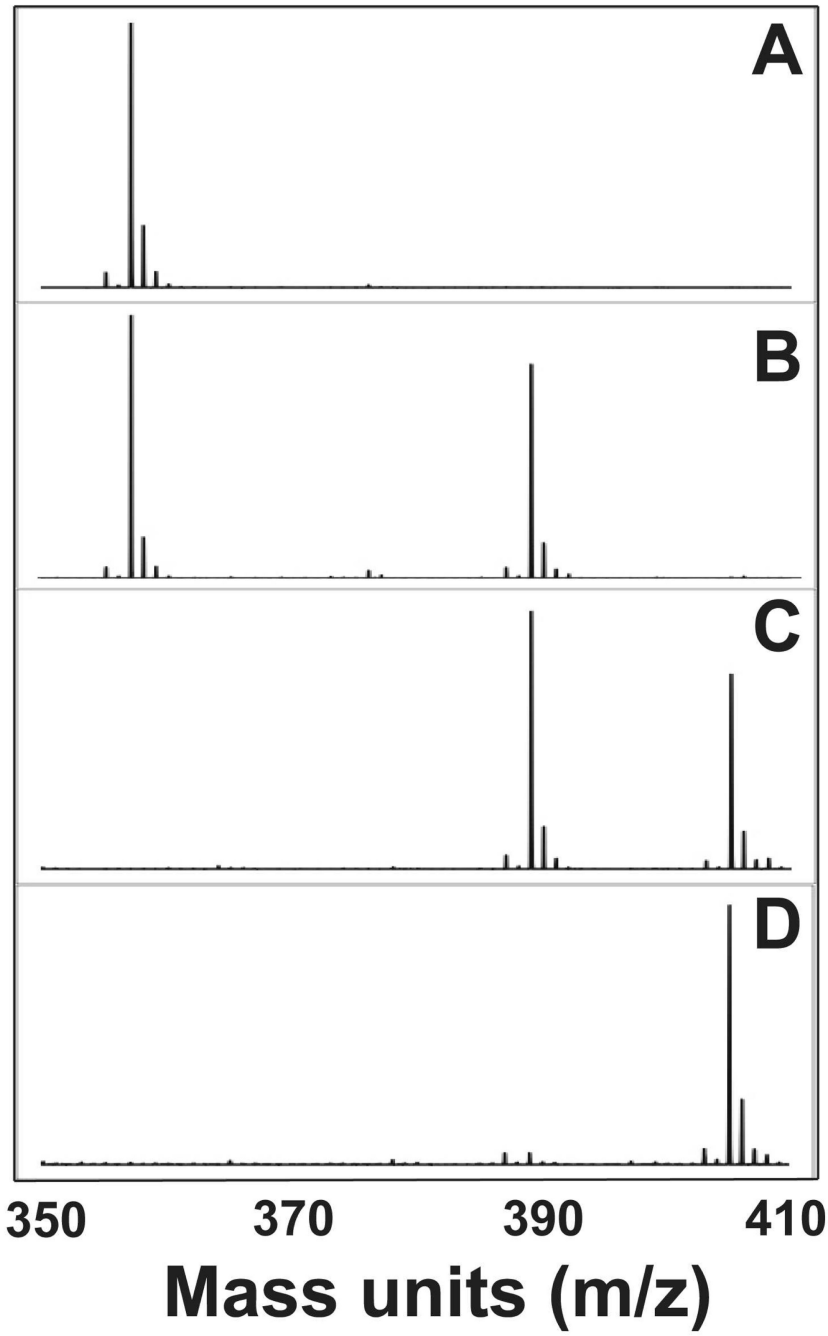

Figure 4.
ESI-MS spectra following the conversion of **1** (*m/z* = 357.1) to **3** (389.2) and **4** (405.2): (A) **1**; (B) **1** + 1 equiv. *m*-CPBA; (C) **1** + 2 equiv. *m*-CPBA; (D) **1** + 3 equiv. *m*-CPBA

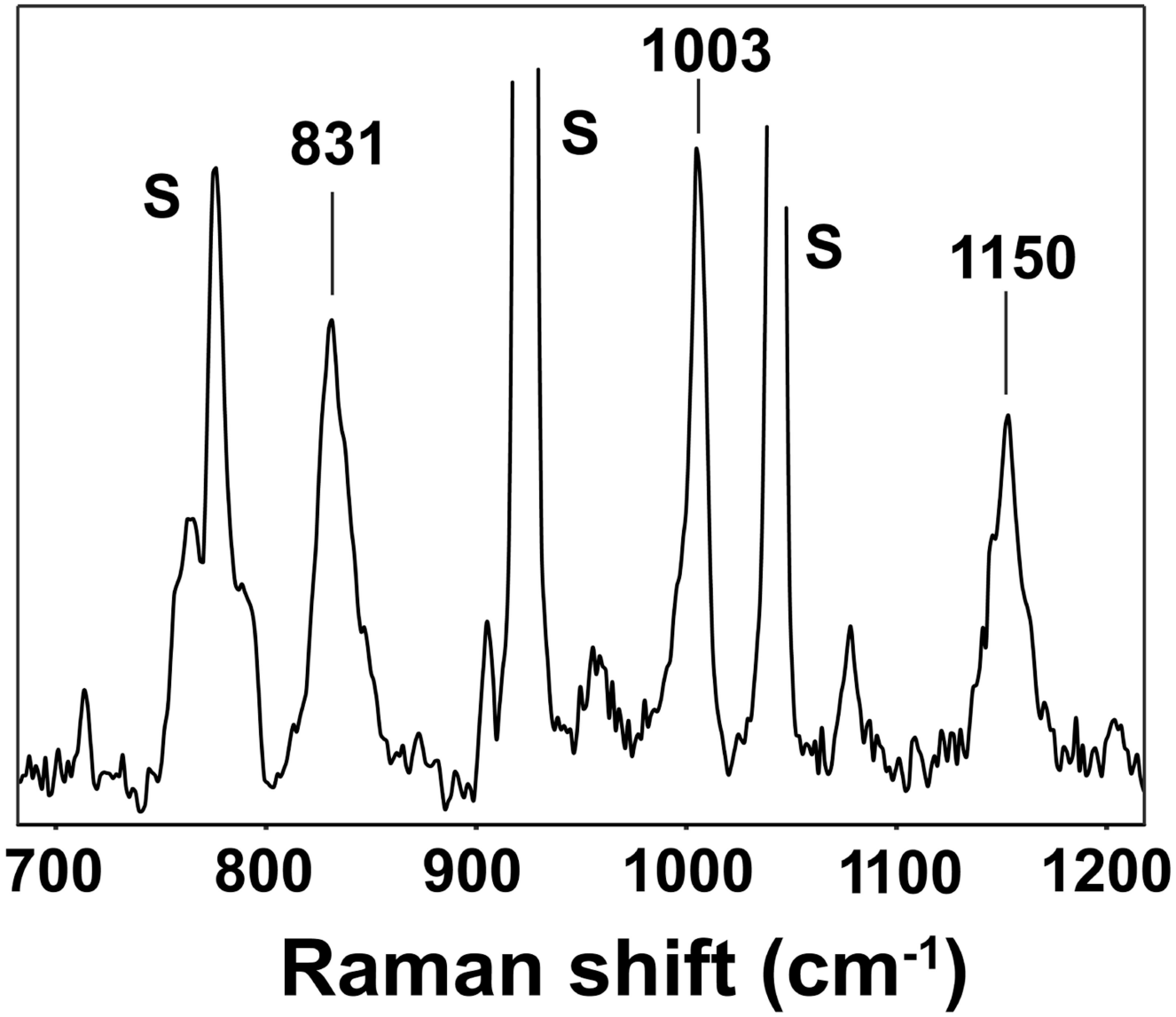

Figure 5.
Resonance Raman spectrum of **4** obtained from an 8 mM CH_3CN frozen solution of **4** using 406.7 nm excitation (10 mW power, 32 scans of 16 s each). S = solvent peak.

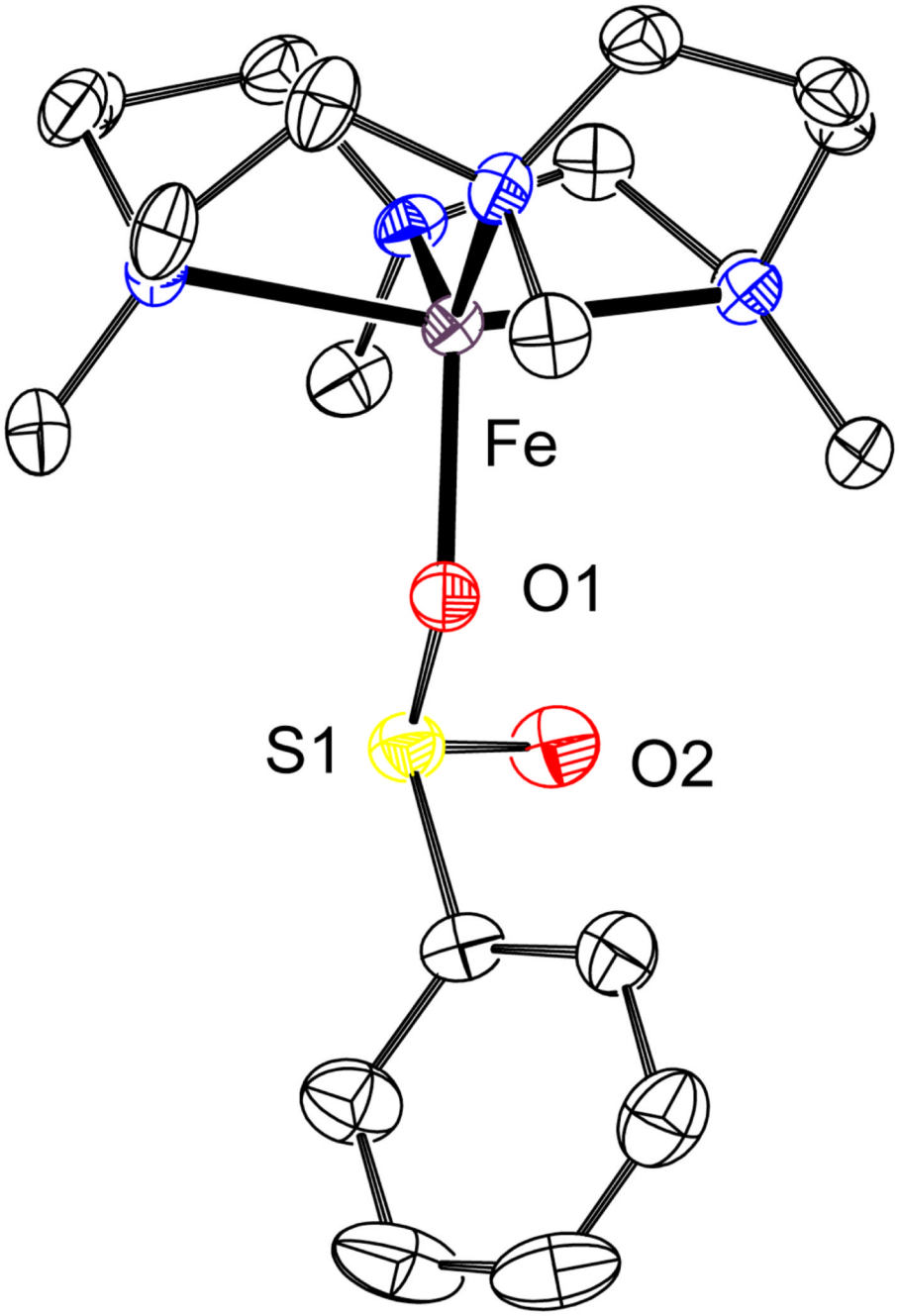

Figure 6.
ORTEP plot of **6** (50% probability level). Hydrogen atoms and the O_2SPh counteranion omitted for clarity. Selected inter-atomic distances (Å): Fe–O1, 1.996(2); Fe–S1, 3.1749(9); Fe–S2, 5.3605(11).

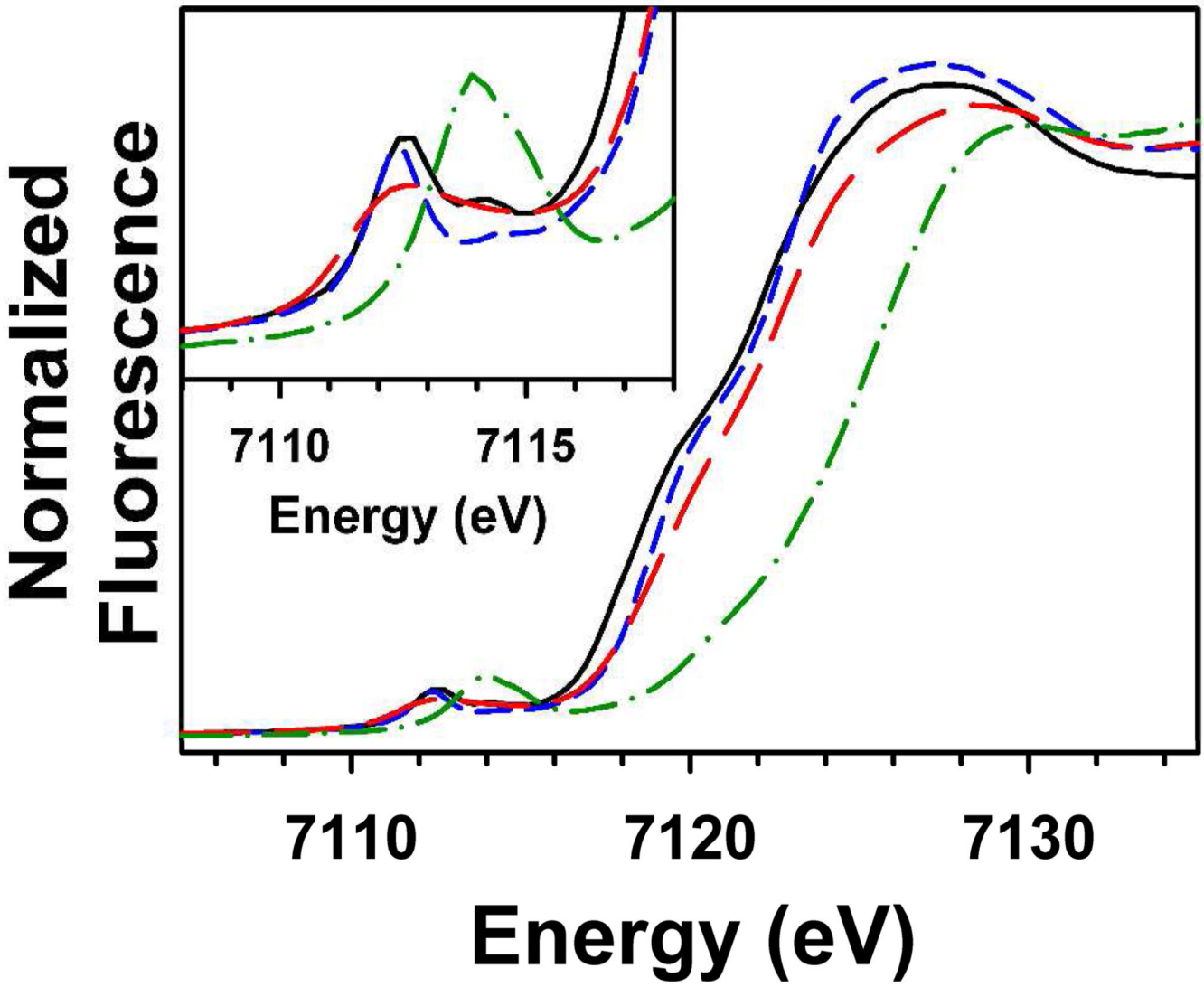

Figure 7.
Comparison of the Fe K-edge X-ray absorption edge and pre-edge (inset) features of species **1** (black, ——), **3** (red, – – –), **4** (green, —·—·—), and **6** (blue, — — —).

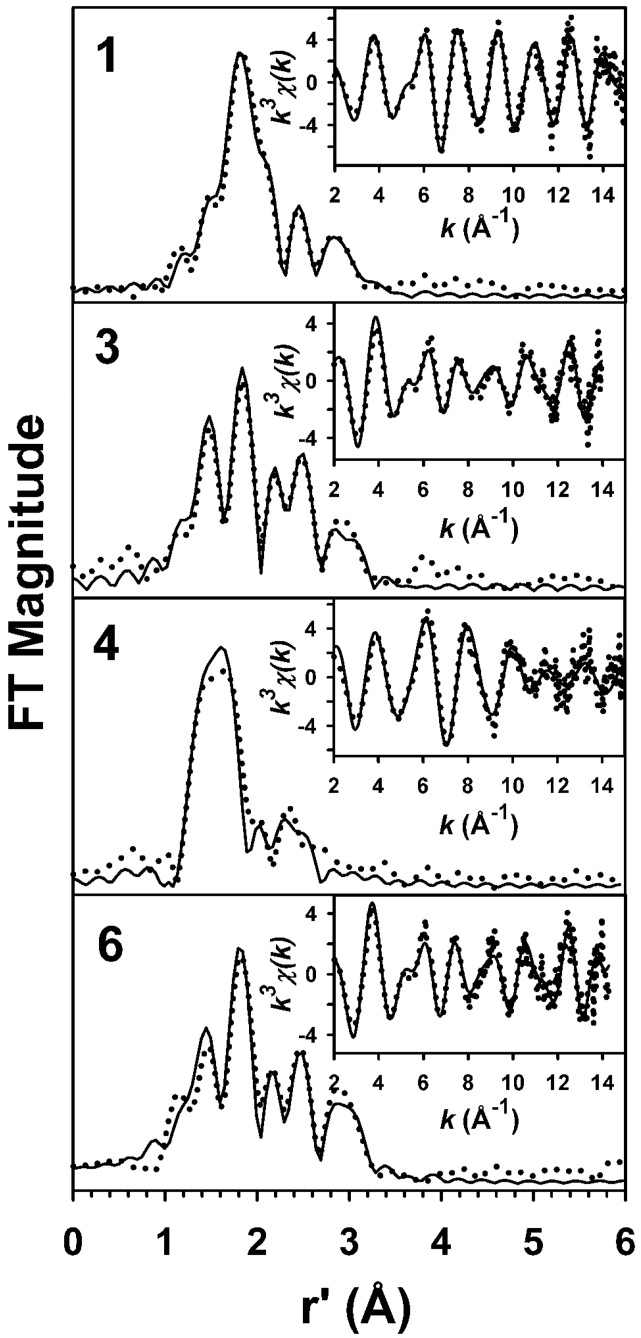

Figure 8.

Fourier transforms of the Fe K-edge EXAFS data ($k^3\chi(k)$) and unfiltered EXAFS spectra ($k^3\chi(k)$, inset) obtained for **1, 3, 4**, and **6**. Experimental data is shown with dotted lines (•••••), while fits are shown with solid lines (——). Fourier transformation ranges are as follows: $k = 2 – 15$ Å^{-1} (**1**), $k = 2 – 14$ Å^{-1} (**3**), $k = 2 – 14.95$ Å^{-1} (**4**), $k = 2 – 14.3$ Å^{-1} (**6**). Fit parameters are shown in bold italics in Table 4.

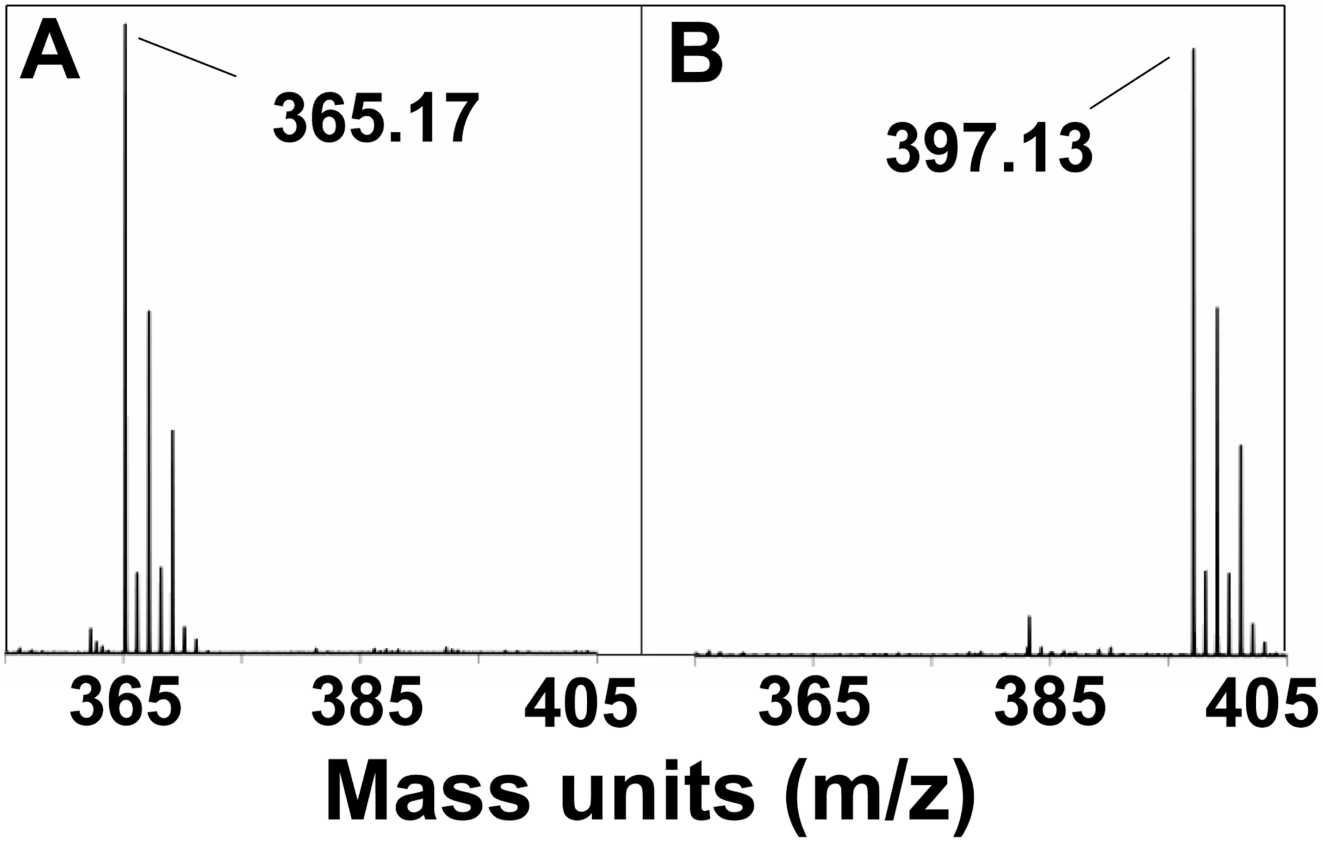

Figure 9.
ESI-MS spectra of compound **7** (A) and after reaction with 2 equiv. *m*-CPBA (B).

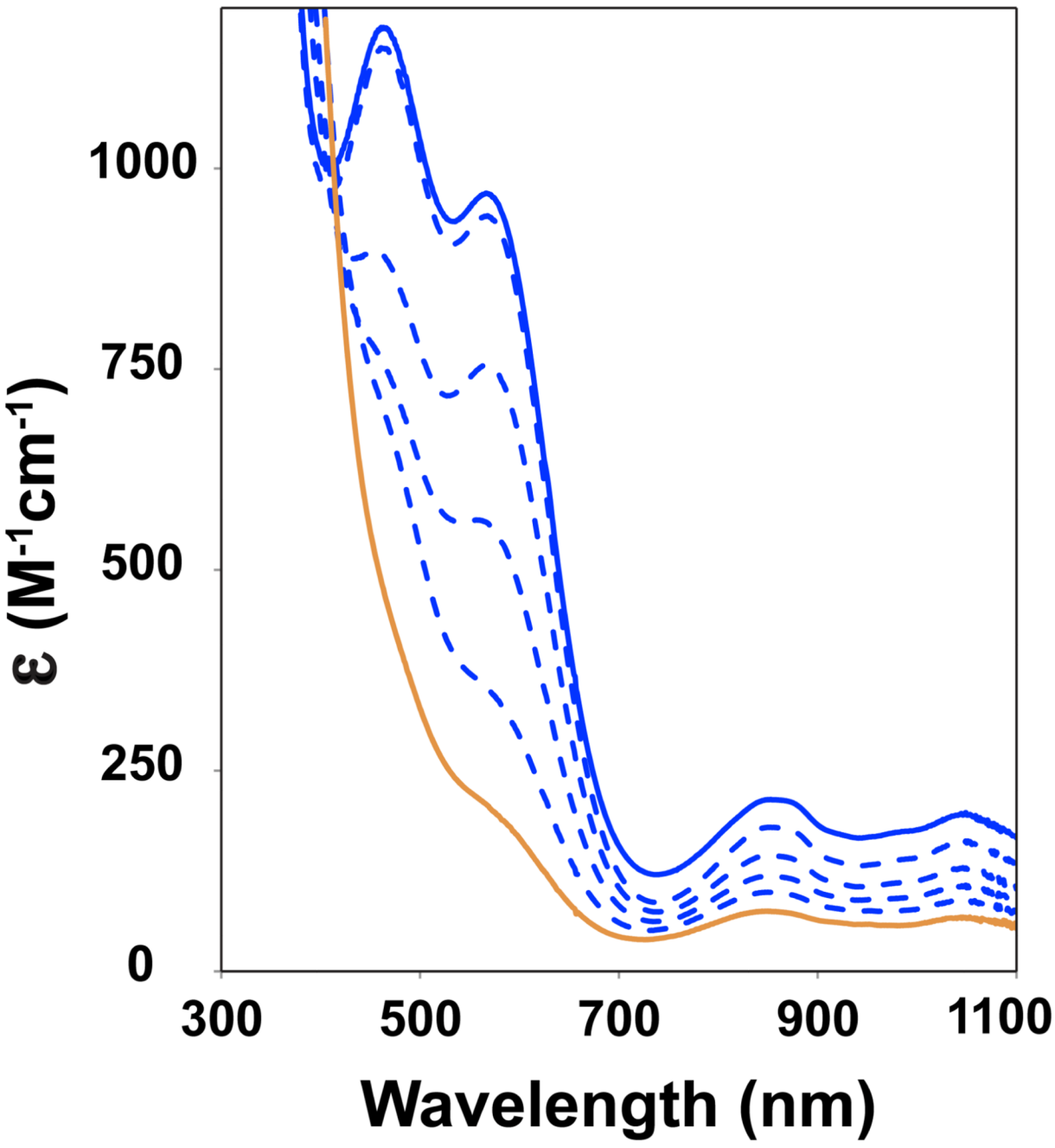

Figure 10.
UV-vis spectral changes observed in the reaction of **2** (0.5 mmol/L, blue solid line) with 6 equivalents $PhCO_2H$ in MeOH at −20 °C over a 3-min period yielding a mixture of compounds **3** and **5** (yellow solid line).

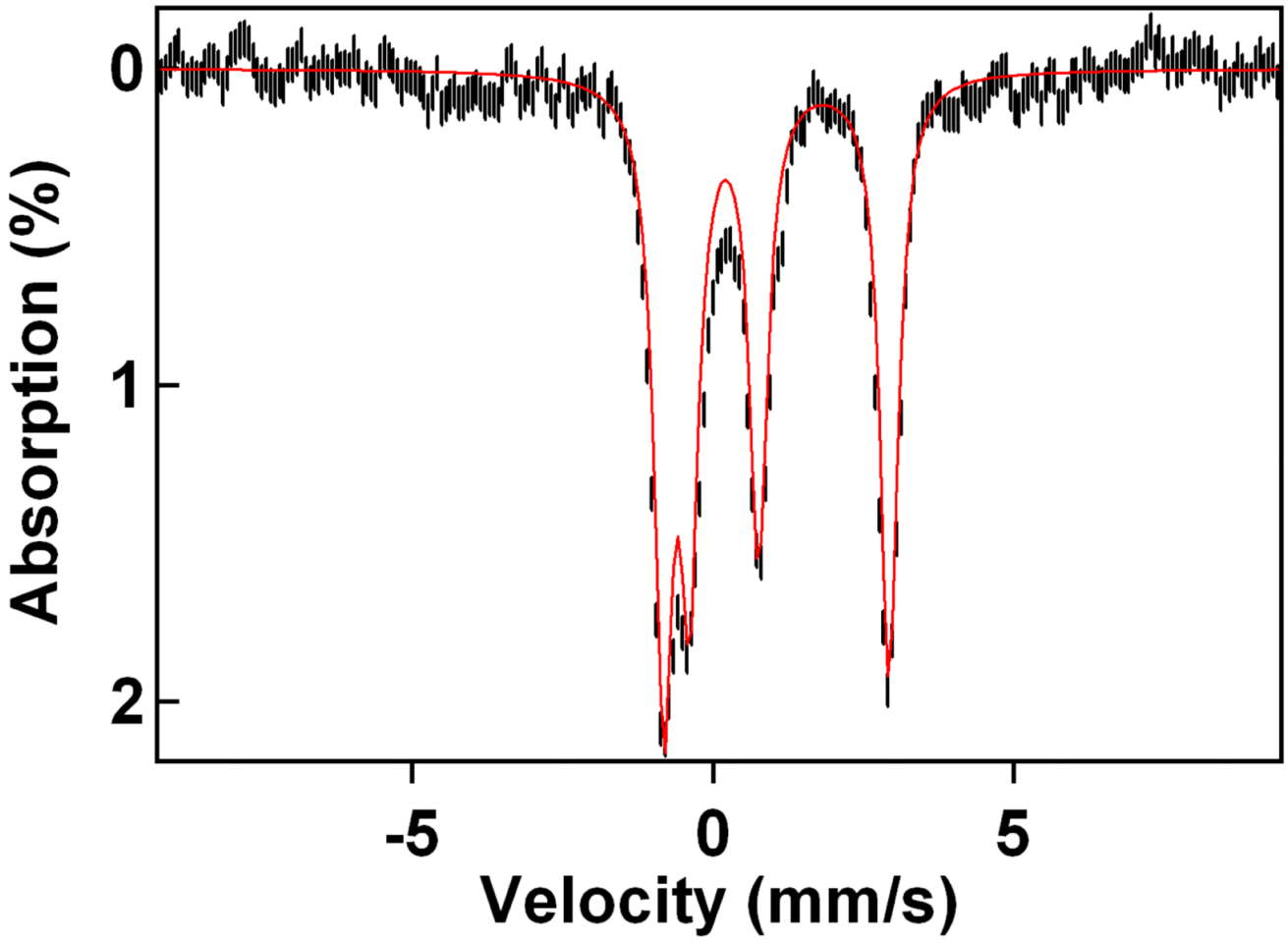

Figure 11.

4.2 K Mössbauer spectrum obtained after adding ~6 equivalents pyridinium triflate at −40 °C to 1.3 mM **2**. 38% of the iron belongs to complex **5** and 47% to **3**; the remainder of the iron belongs to broad and unresolved Fe^{III} species.

1, $[Fe^{II}(TMCS)]^{+}$ **2**, $[Fe^{IV}(O)(TMCS)]^{+}$

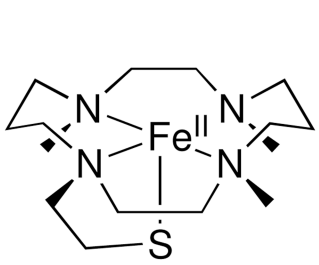

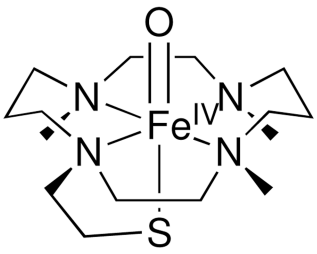

$[Fe^{IV}(O)(TMC)(X/Y)]^{2+/+}$ $[Fe^{IV}(O)(TPA)(X)]^{2+/+}$

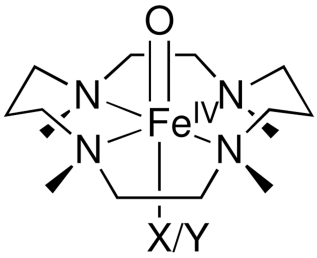

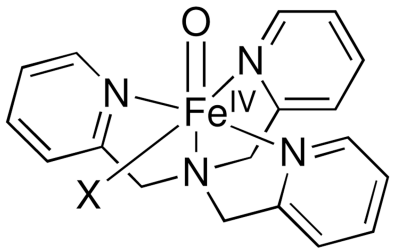

$X = CH_3CN, Cl, CF_3CO_2; Y = N_3, NCS$

$[Fe^{IV}(O)(N4Py)]^{2+}$

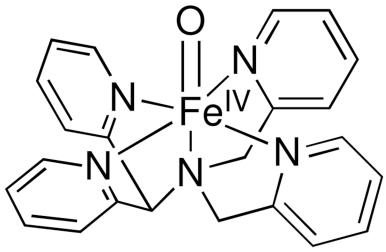

Scheme 1.
Structures of **1, 2**, and some synthetic oxoiron(IV) complexes (TMC, TPA, N4Py).

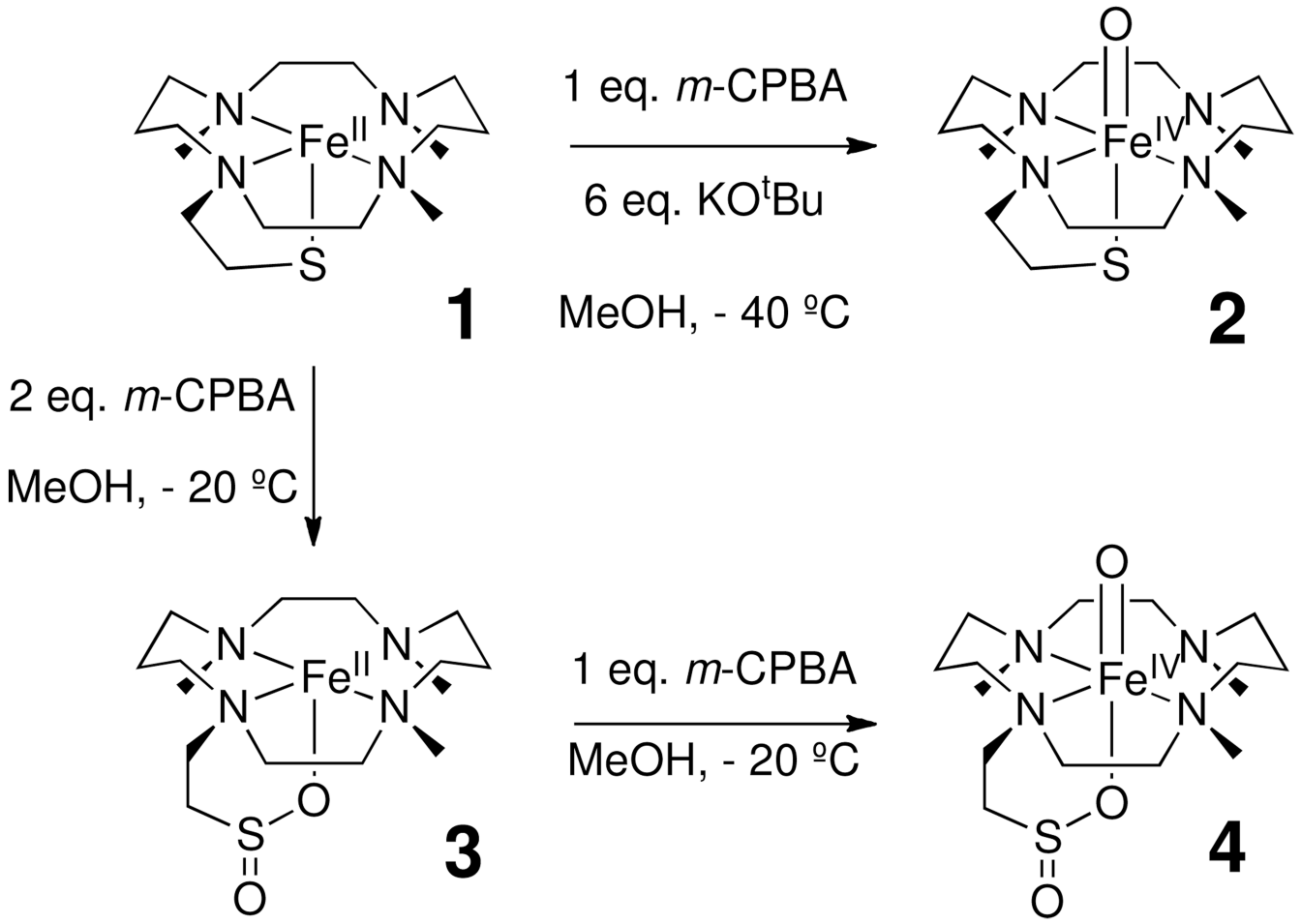

Scheme 2.
Reaction of **1** with *m*-CPBA.

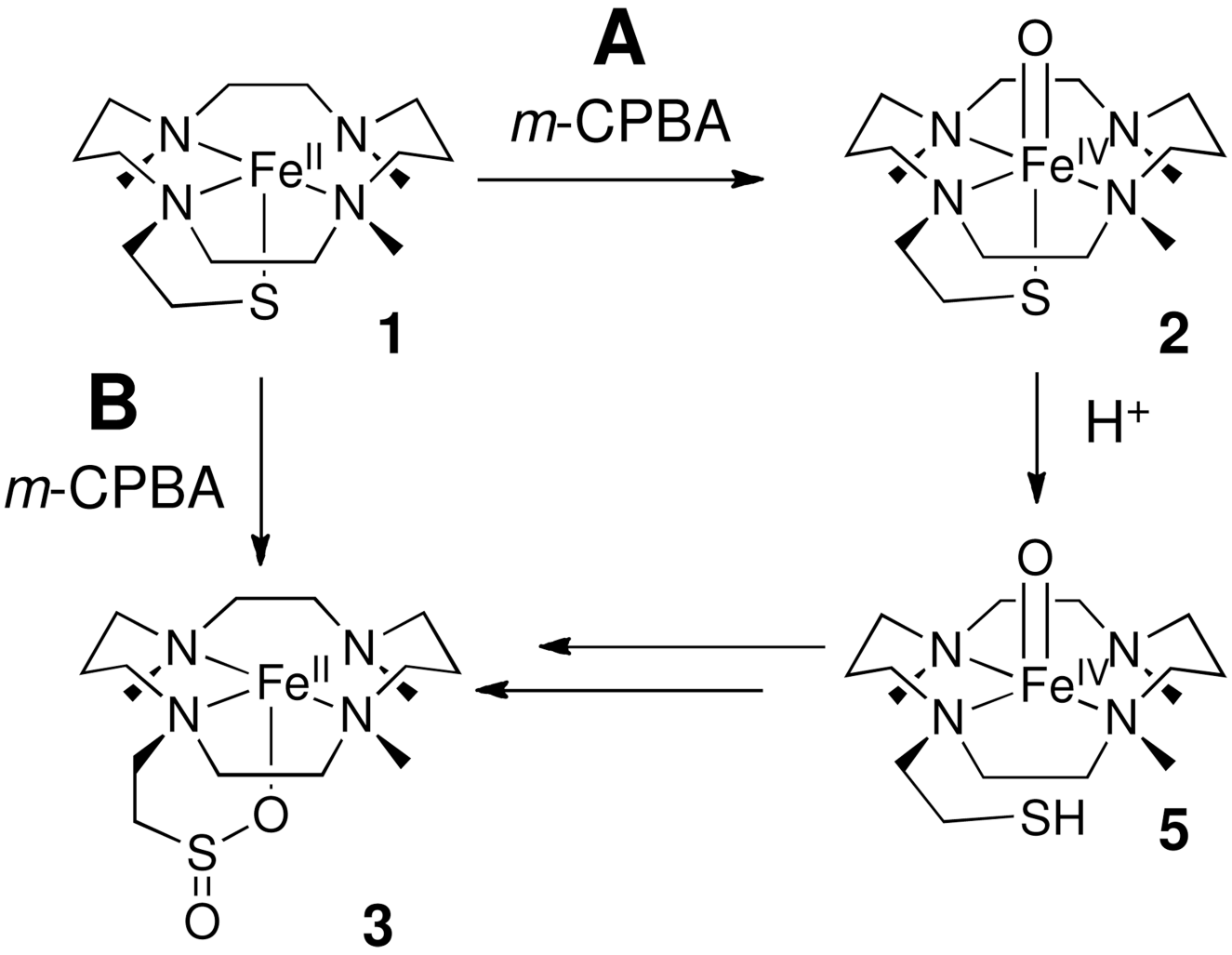

Scheme 3.

Postulated mechanism for the conversion of **1** to **3** in the reaction between **1** and *m*-CPBA without added base. *m*-CPBA could react either at the iron site (pathway A) or the sulfur site (pathway B) of **1**, evidence for both pathways is provided.

Table 1

Crystal data and structure refinement for **6**

Empirical formula	$C_{26}H_{42}FeN_4O_4S_2$	
Formula weight	594.61	
Temperature	173(2)K	
Crystal system	Orthorhombic	
Space group	$P2_12_12_1$	
Unit cell dimensions	a = 8.8119(14) Å	α = 90°
	b = 12.913(2) Å	β = 90°
	c = 24.946(4) Å	γ = 90°
Volume	2838.6(8) $Å^3$	
Z	4	
Density (calculated)	1.391 mg/m^3	
Crystal color, morphology	Colorless, Plate	
Crystal size	0.45 × 0.42 × 0.08 mm^3	
Goodness-of-fit on F^2	1.068	
Final R indices [I > 2sigma(I)]	$R1$ = 0.0382, $wR2$ = 0.0765	
R indices (all data)	$R1$ = 0.0487, $wR2$ = 0.0798	
Absolute structure parameter	−0.026(15)	

Table 2

Physical properties of **1** – **6** and related [Fe^{IV}(O)(TMC)(**X**)] complexes.

	λ_{max} (nm) (ε (M^{-1} cm^{-1}))	δ^a (mm/s)	$\Delta E_Q{}^a$ (mm/s)	$\nu_{Fe=0}$ (cm^{-1})	Pre-Edge Area	Edge Energy (eV)
1	320 (1500)	0.90	3.06	-	13.6, 3.6	7122.4
2[b]	460 (1300), 570 (1200), 860 (200), 990 (150)	0.18	0.21	n.d.	20.0	7125.1
3	280 (3000)	1.01	3.77	-	13.4	7123.0
4	830 (170), 990 (170)	0.19	1.28	831	31.0	7125.6
5	830 (~150), 1000 (~150)	0.16	1.15	n.d.	n.d.	n.d.
6	230 (2500), 270 (1700)	1.13	3.92	-	8.3, 1.5	7123.1
[Fe^{IV}(O)(TMC)(**X**)][c]						
$^-$**CN**	858 (250)	0.15	0.25	823	21.0	7124.8
$^-$**O$_2$CCF$_3$**	836 (250)	0.20	1.39	854	30.9	7124.0
NCCH$_3$	824 (400)	0.17	1.23	839	26.2	7124.5

[a] Estimated uncertainties for Mössbauer parameters are as follows: δ: ± 0.01 mm/s, ΔE_Q: ± 0.05 mm/s.

[b] Data from Ref. 19.

[c] Data from Ref. 21(d). n.d. = not determined

J Am Chem Soc. Author manuscript; available in PMC 2012 May 10.

Table 3

Selected Fe–O/S/N distances (Å) in species **1–4**, and **6**.

	Fe–O	Fe–S	Fe=O	Fe–N
1[a/b]	-	2.297(3)[a]	-	2.176(5), 2.225(5)[a]
		2.29[b]		4 @ 2.19[b]
2[b]	-	2.33	1.70	3 @ 2.09
3[b]	1.95	3.27	-	3 @ 2.19
4[b]	-	-	1.64	4 @ 2.05
6[a/b]	1.996(2)[a]	3.1749(9) [a]	-	2.176(2), 2.196(2), 2.231(2), 2.257(2)[a]
	1.95[b]	3.28[b]		4 @ 2.18[b]

[a] from X-ray crystallography.

[b] from EXAFS analysis.

Table 4

Selected EXAFS Fitting Results for Species **1**, **3**, **4**, and **6**.[a]

		Fe–N/O			Fe-O/N			Fe•••S			Fe•••C			
Species	**fit**	**n**	***r***	**σ^2**	**n**	***r***	**σ^2**	**n**	***r***	**σ^2**	**n**	**r**	**σ^2**	***F*[b]**
1	1	5	2.18	1.6										0.506
	2	6	2.18	2.6										0.558
	3	4	2.19	2.2				1	2.29	2.6				0.436
	4	4	2.19	2.1				1	2.29	2.7	5	3.07	9.7	0.389
											4	***2.99***	***2.3***	
	5	***4***	***2.19***	***2.2***				***1***	***2.29***	***2.2***	***4***	***3.16***	***1.0***	***0.312***
											6	***3.54***	***8.1***	
3	1	4	2.21	11.8										0.754
	2	5	2.22	24.5										0.770
	3	3	2.19	3.1	1	1.97	1.1							0.582
	4	4	2.19	5.8	1	1.95	0.7							0.605
	5	3	2.19	3.3	1	1.96	1.2	1	3.27	5.5				0.507
	6	*3*	***2.18***	***3.5***	*1*	***195***	***0.8***	***1***	***3.27***	***2.9***	***4***	***2.97***	***4.6***	***0.378***
4	1	4	2.07	3.8										0.529
	2	5	2.07	5.1										0.531
	3	5	2.06	5.3	1	1.64	4.2							0.443
	4	5	2.06	5.2	0.8[c]	1.64	2.7							0.430
	5	***5***	***2.06***	***5.2***	***0.8***[c]	***1.64***	***2.7***				***4***	***2.96***	***9.3***	***0.411***
6	1	5	2.20	10.4										0.717
	2	4	2.20	4.2	1	1.96	2.3							0.593
	3	4	2.20	4.4	1	1.96	1.9	1	3.29	1.4				0.492
	4	***4***	***2.18***	***4.5***	***1***	***1.95***	***13***	***1***	***3.28***	***0.7***	***4***	***2.99***	***4.3***	***0.402***
	5	4	2.18	4.7	1	1.95	1.7				4	2.98	1.6	0.467
											4	3.16	1.4	

[a]Fourier transform ranges: **1** k = 2.0 – 15 Å^{-1} (resolution = 0.12 Å), **3**, k = 2.0 – 14 Å^{-1} (resolution = 0.13 Å), **4**, k = 2.0 – 14.95 Å^{-1} (resolution = 0.12 Å), **5**, k = 2.0 – 14.3 Å^{-1} (resolution = 0.13 Å). r is in units of Å; σ^2 is in units of 10^{-3} Å^2. All fits are to unfiltered data.

[b] Goodness-of-fit parameter F defined as $[\Sigma k^6(\chi_{exPt1}-\chi_{calc})^2 / \Sigma k^6 \chi_{exPt1}^2]^{1/2}$

[c] The value of n for the 1.64-Å shell was fixed at 0.8 for fits 4–4 and 4–5 in view of the fact that the sample was found to contain 80% **4** by UV/Vis spectroscopy.

Table 5

Reactivity towards PPh_3 and DHA[a]

	PPh_3 (k_2, $M^{-1}s^{-1}$)	**DHA (k_2, $M^{-1}s^{-1}$)**
2[b]	0.016[b]	7.5[b]
4[b]	12.2 ± 0.3[c]	3.5 ± 0.1[d]
$[Fe^{IV}(O)(TMC)(NCCH_3)]^{2+}$	5.5 ± 0.3[c]	0.20[b]

[a] Carried out at 0 °C in 1:1 MeOH/CH_3CN.

[b] from ref. 21c.

[c] $OPPh_3$ was obtained in quantitative yield relative to Fe^{IV}=O.

[d] Anthracene was obtained in 40% yield relative to Fe^{IV}=O.